Study of the dipole giant resonance in $(\gamma,x\gamma')$ experiments

B. S. Ishkhanov and I. M. Kapitonov
Nuclear Physics Institute, Moscow State University, Moscow

R. A. Éramzhyan
Institute of Nuclear Research, Russian Academy of Sciences, Moscow

Fiz. Elem. Chastits At. Yadra **23**, 1770–1826 (November–December 1992)

The $(\gamma,x\gamma')$ experiments in which a photon γ' is recorded and its energy measured, and x is an unobserved particle emitted from the nucleus (a proton, neutron, deuteron, etc.), are described. The use of germanium detectors with large sensitive volume (~ 100 cm^3) in these experiments for the detection and spectrometry of the photon γ' significantly increases the information about the partial nuclear photodisintegration channels, particularly in (γ,p_f) and (γ,n_f) reactions, where f numbers the levels of the final nucleus. It also becomes possible to gain greater understanding of the mechanism for the formation and decay of the dipole giant resonance. The technique and reliability of such experiments are discussed in this review, along with the principles for interpreting them and specific physical results. The importance of combined analysis of the data from $(\gamma,x\gamma')$ experiments and particle spectrometry experiments is stressed. The data for the ^{24}Mg, ^{27}Al, and ^{40}Ca nuclei are discussed in detail.

INTRODUCTION

The dipole giant resonance (DGR) is one of the fundamental nuclear excitation modes. The nearly fifty years of study of this mode have played a decisive role in forming the contemporary ideas about collective excitations in nuclei. The various approaches developed for describing it have mainly been directed toward the interpretation of the average resonance characteristics: the localization region and its shape and width. The corresponding experimental data is usually taken either from the data on the total photoabsorption cross section or from the data on the total photoproton and photoneutron cross section. In the case of transuranium elements it is taken from the data on the fission cross section.

However, the DGR decay characteristics, particularly if the states of the final nucleus [the so-called partial disintegration channels (γ,x_f), where x is the emitted particle and the subscript f refers to a certain state of the final nucleus] are fixed, contain more detailed information about the nature of the giant resonance.[1,2] This is primarily information about how the energy concentrated in the dipole state is distributed. This essentially corresponds to the relation between the widths of the distribution of the doorway dipole states over complicated states, leading to loss of collectivity, and the widths of nucleon emission into the continuum at each stage of complexification of the configuration. The different nucleon emission stages are referred to as the semidirect, preequilibrium, and equilibrium processes.

The *semidirect* process is the process of nucleon emission from the DGR into the continuum, with the final nucleus remaining in a hole state. These hole states of the final nucleus are well known from the reactions (p,d), $(d,^3\mathrm{He})$, and so on. The partial transitions to these hole states carry information about the doorway particle–hole configurations and are therefore very interesting.

The *preequilibrium* decay of the DGR is related to nucleon emission into the continuum during later but still early stages of the spread of the doorway dipole states. States of the final nucleus which are more complicated than hole states are populated as a result of the nucleon emission. However, these states are still not very complicated; their nature is known, so that it is possible to tell at what stage of the spread of the doorway states the nucleon emission occurred. Therefore, the study of the partial photodisintegration channels of nuclei makes it possible to reconstruct the microscopic picture of the entire phenomenon of the photonuclear giant resonance. This is the reason for the recent great interest in studying the partial DGR decay channels. As far as *equilibrium* decay is concerned, it no longer contains information about the initial stage and mainly reflects the average characteristics of the nuclear system.

The decay characteristics of DGRs in light ($A<40$) and intermediate nuclei are of particular interest. In light nuclei no single peak appears, owing to the incomplete collectivization of the particle–hole configurations. The dipole transitions of nucleons from various subshells are concentrated in different energy regions. The resonance is "dispersed" among several energetically allowed groups of local dipole transitions. There is also the so-called *configuration splitting* of the DGR, which determines the main features of the resonance in these nuclei. The information on the microscopic structure of local resonances is concentrated in the cross sections for semidirect processes.

The phenomenon of configuration splitting is discussed in detail in the review of Ref. 2. In light nuclei the bulk of the DGR is essentially formed from nucleon transitions of two types:

- Type A: transitions from an outer shell to a free state (for nuclei of the $1d2s$ shell these are $1d2s \rightarrow 1f2p$ transitions);
- Type B: transitions from an internal filled shell to an

 0090-4759/92/060774-25$04.00

outer partially filled shell (for nuclei of the $1d2s$ shell these are $1p \rightarrow 1d2s$ transitions).

The energies of these transitions differ strongly, owing to the abrupt drop of deep single-particle levels. Owing to the strong energy spread, a single dipole state is not formed in these nuclei and the DGR essentially remains dispersed over strongly separated, individual groups of particle–hole states, from which local dipole states can be formed.

In nuclei of the $1d2s$ shell the dipole substates pertaining to transitions of type A populate, as a result of the semidirect decay mechanism, hole states with $l=0$ and 2, the parity of which is positive. The substates pertaining to type-B transitions populate hole states with $l=1$, the parity of which is negative.

Knowing the fraction of semidirect nucleons and the quantum numbers of the populated hole states of the final nucleus, it is possible to separate the two types of substates forming DGRs and to extract quantitative information about the magnitude of the effect.

Strictly speaking, owing to the incomplete collectivization, the part of the resonance directly related to type-A transitions is also split. Therefore, the form of the energy dependence of the cross section in the partial transitions depends on what hole state of the final nucleus is populated. However, the available direct experimental data are still rather sparse, and the accuracy is not good enough to form a qualitative judgment about this aspect of the problem of configuration splitting. Therefore, in what follows we shall discuss a more global effect related to the splitting of transitions from the outer and inner shells.

Furthermore, in nuclei with $N \neq Z$ the dipole resonance consists of two isospin branches, $T=T_0$ and $T=T_0+1$, where T_0 is the isospin of the ground state of the initial nucleus. These branches are collectivized differently. It is interesting to study them separately. The branches can be separated only by analyzing the partial cross sections. This problem is closely intertwined with that of the isospin purity of the dipole states.

This is a far from complete list of problems related to the study of nucleon emission into the continuum. An exhaustive theoretical interpretation of the phenomenon of the spreading of doorway dipole states among more complicated states and the emission of a nucleon into the continuum at each stage has not yet been given. At present, the theory consists of various model representations which are fairly simple and clear. On the whole, they permit a quantitative analysis of the experimental data and allow the contribution of semidirect processes and the role of various configurations in dipole-resonance formation in different energy regions to be judged.

In this review we discuss the methods of measuring the partial photonucleon cross sections for the example of three nuclei (^{24}Mg, ^{27}Al, and ^{40}Ca). We study the corresponding experimental data and carry out a theoretical analysis with the goal of explaining semidirect processes and the microscopic structure of the dipole resonance.

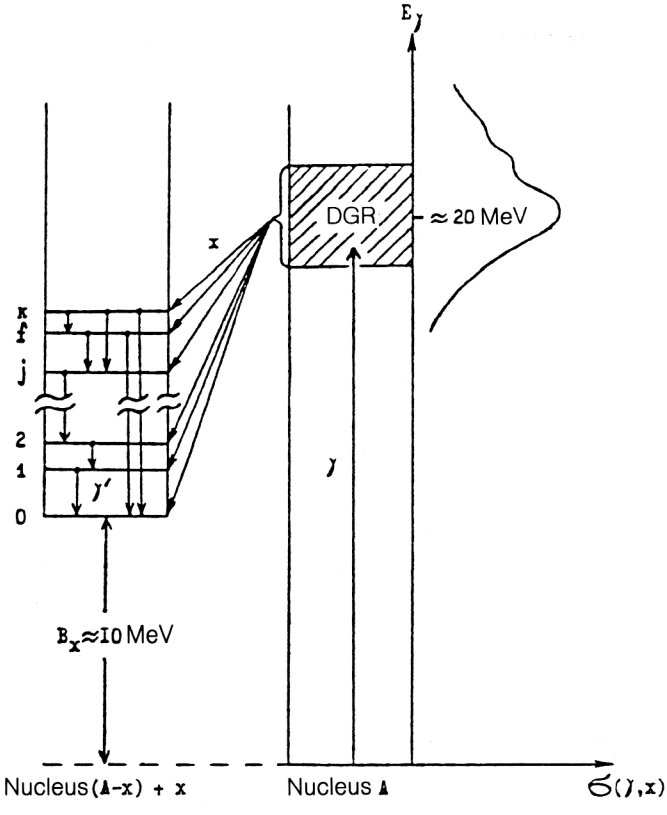

FIG. 1. Decay of a dipole giant resonance (DGR) with population of individual levels of the final nucleus.

1. METHODS OF MEASURING THE PARTIAL CROSS SECTIONS USING THE BREMSSTRAHLUNG SPECTRUM IN NUCLEAR PHOTODISINTEGRATION

Data on the partial photodisintegration channels are obtained in two types of experiment (see Fig. 1). One measures either the spectra of the emitted particles x or the spectra of the γ quanta reducing the excitation of the final nuclear states populated as a result of emission of the particle x. Experiments of the first type are referred to as particle *spectrometry*, and those of the second are called $(\gamma,x\gamma')$ *experiments*.

The partial cross sections extracted from the spectra of particles x, especially when these particles are nucleons, are known with high statistical accuracy, and intermediate structure is clearly observed in them. Information about the angular momentum of the emitted particle is extracted from the data on the nucleon angular distributions. However, in such experiments, which are usually carried out in bremsstrahlung-radiation beams, it is impossible to separate the partial channels of the processes leading to the population of states of the final nuclei when the difference of the binding energies is smaller than the step with which the upper limit of the bremsstrahlung-radiation spectrum varies.

The use in $(\gamma,x\gamma')$ experiments of semiconductor Ge(Li) detectors, which have high energy resolution, permits the separation of the partial photodisintegration channels corresponding to the population of closely spaced states of the final nuclei. An advantage of the method is

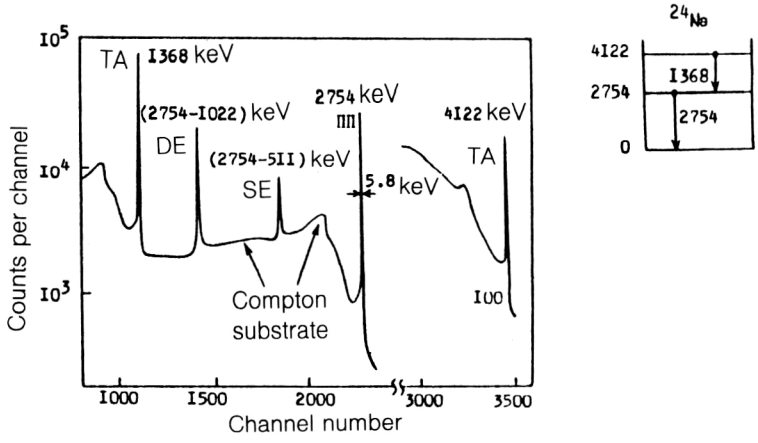

FIG. 2. Spectrum of γ quanta from a ^{24}Na source obtained using a Ge(Li) detector of volume 85 cm^3 (Ref. 11). In the upper right-hand corner we show the γ-transition scheme for ^{24}Na.

that it permits the simultaneous study of photodisintegration channels corresponding to the emission of particles of different type. A drawback of $(\gamma,x\gamma')$ experiments is the statistical accuracy, which is low compared with that of the data extracted from the x spectra. This makes it difficult to measure the energy dependences of the partial cross sections and the angular distributions of the photons γ'. Another drawback is the need for good knowledge of the branching ratios of the γ transitions. In these experiments it is impossible to obtain information about the population of the ground states of the final nuclei and states whose energy is considerably higher than the nucleon separation energy in the final nucleus. However, the fact that in $(\gamma,x\gamma')$ experiments it is possible to determine the individual partial channels makes these experiments an effective method of studying nuclear photodisintegration. The *simultaneous* use of the results of measurements carried out by these two methods can greatly advance the understanding of DGRs at the microscopic level.

The data from 39 years of $(\gamma,x\gamma')$ experiments carried out using Ge(Li) detectors were published in 1966. The results of the 32 studies published through 1984 were systematized in Ref. 3. Seven more publications appeared later.[4–10] All the publications are devoted to the study of light nuclei ($A<40$–50) and, with one exception, pertain to the dipole-giant-resonance region. Most of the experiments (22 of them) were carried out for nuclei of the $1d2s$ shell ($16<A\leqslant 40$). Unfortunately, for most of the transitions it was not possible to measure the energy dependence of the $(\gamma,x\gamma')$ cross section. Only the cross sections integrated over the giant resonance region were measured, and we shall work with them.

The present review is based on this last group of studies. It is for nuclei of the $1d2s$ shell that $(\gamma,x\gamma')$ experiments have given the most valuable information, which, together with the independent results of studying the partial photonuclear reactions in particle spectrometry experiments, now make it possible to arrive at a number of important conclusions about the nature of DGRs of nuclei with $16<A\leqslant 40$.

In analyzing $(\gamma,x\gamma')$ experiments we concentrate on the single-nucleon partial channels ($x=p$ or n) via which a dipole resonance in this range of nuclei usually decays. We do not consider less intense channels leading to the emission of two or more nucleons ($x=np$, $2p$, $2n$, etc.) or complex particles ($x=d$, τ, α, etc.). The information on them for nuclei of the $1d2s$ shell is still too sparse and disconnected for systematization to be carried out.

2. THE EXPERIMENTAL SETUP AND ANALYSIS OF EXPERIMENTAL DATA ON γ DEEXCITATION OF THE FINAL NUCLEI PRODUCED IN DGR DECAY

The nucleon-spectrometry setups are quite familiar. There is therefore no need to dwell on this subject. The setups for measuring the γ deexcitation of daughter-nucleus states populated as a result of the decay of a photonuclear dipole resonance have not been as completely described. To fill this gap, we begin with a description of the principles of operation of such a setup as a whole and its various elements.

The central element of the setup recording γ' quanta in $(\gamma,x\gamma')$ experiments is a Ge(Li) detector of large sensitive volume (usually 30–100 cm^3). For photon energies in the most interesting range 1–10 MeV the energy resolution of the best Ge(Li) detectors is 0.1–0.2%. This means that such detectors can be used in this energy range to distinguish nuclear γ transitions separated by a few keV. For light nuclei ($A<40$–50) the energy resolution attained makes it possible to distinguish most of the γ transitions (when their intensity is not too low).

The response function of the Ge(Li) spectrometer is rather complicated. For $E_\gamma>2m_ec^2$ ($m_ec^2=0.511$ MeV) it consists of three narrow lines with energies E_γ, $E_\gamma-m_ec^2$, and $E_\gamma-2m_ec^2$, superimposed on the continuous distribution of recoil Compton electrons. In Fig. 2 we show the γ spectrum from a ^{24}Na source obtained using a coaxial Ge(Li) detector of volume 85 cm^3 (Ref. 11). The three middle peaks correspond to the detection of γ quanta with energy 2.754 MeV (the γ-transition scheme for ^{24}Na is given in the upper right-hand corner of Fig. 2). Of these, the right-hand peak is the total-absorption (TA) peak formed by the photoeffect, e^-e^+ pair creation with subsequent detection of two photons of energy 0.511 MeV from positron annihilation, and also multiple Compton scattering with subsequent absorption. The main contribution to

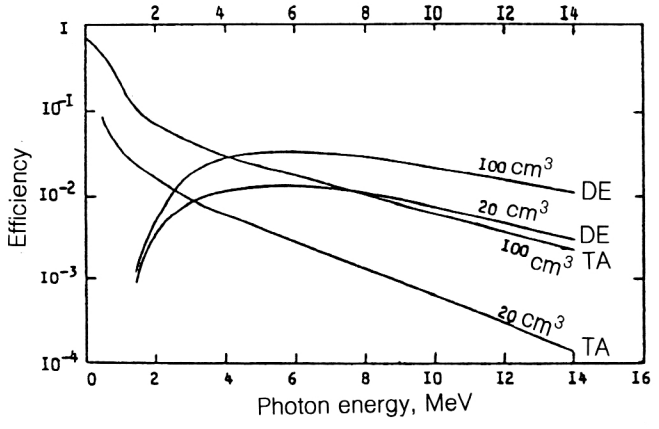

FIG. 3. Efficiency of γ detection using the peaks corresponding to total absorption (TA) and double emission (DE) of annihilation photons for two Ge(Li) detectors of volume 20 and 100 cm^3.

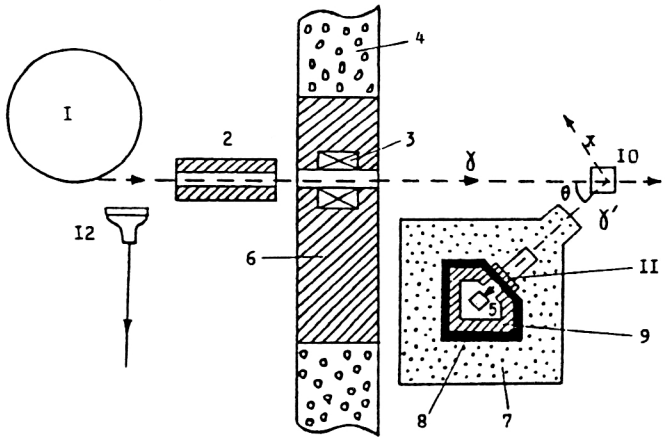

FIG. 4. Setup of the $(\gamma,x\gamma')$ experiment (details given in the text).

the total-absorption peak comes from the first of these effects. The peaks with energies 2.754–0.511 MeV and 2.754–1.022 MeV therefore correspond to cases where one or both of the annihilation photons leaves the sensitive volume of the detector without being recorded. We shall henceforth refer to these peaks as the *single* and *double* emission of annihilation photons.

The spectrum shown in Fig. 2 also contains a strong peak at 0.511 MeV (not shown) corresponding to the detection of annihilation photons emitted by the materials surrounding the detector.

The peak on the far right of Fig. 2 corresponds to the simultaneous detection of cascade γ quanta (1.368 and 2.754 MeV). Its energy is equal to the sum of the energies 1.368 and 2.754 Mev, and its strength is 0.7% of that of the peak at 2.754 MeV. This means that in $(\gamma,x\gamma')$ experiments, where the statistical accuracy is usually not better than a few percent, peaks corresponding to the simultaneous detection of cascade γ quanta are not distinguishable from the background and therefore do not complicate the spectral distribution.

In Fig. 3 we show the energy dependences of the γ recording efficiency when the peaks corresponding to total absorption (TA) and double emission (DE) of annihilation photons are used for two coaxial Ge(Li) detectors of volume 20 and 100 cm^3. The efficiency curves for the single-emission (SE) peak have the same shape as those for the DE peak, but they are lower by about a factor of 1.5 for a detector of volume 100 cm^3. We see that for $E_\gamma > 4$ MeV the recording efficiency when the DE peak is used is greater than that when the TA peak is used.

The efficiency is quoted relative to that of the standard NaJ spectrometer with a 76.2×76.2-mm cylindrical crystal. We see that for 1-MeV γ quanta the efficiency of a Ge(Li) detector of volume 100 cm^3 is five times greater than that of the NaJ detector.

The $(\gamma,x\gamma')$ experiments are usually carried out in beams of bremsstrahlung γ radiation from electron accelerators. A typical experimental setup is shown in Fig. 4. Since the background conditions are complicated, special measures are taken to ensure careful screening of the detector from external radiation, including low-energy radiation, in order to eliminate the effect of pileup of small-amplitude pulses.

The bremsstrahlung-radiation beam from the accelerator 1 (Fig. 4) before entering the experimental hall passes through a long ($\sim$1 m) lead collimator 2 and cleaning magnet 3. The experimental hall is separated from the accelerator chamber by a concrete wall 4 of thickness 1.5–2 m. A lead shield 6 covers the detector 5 on the accelerator side. The detector is located inside a multilayer shield made of paraffin 7, cadmium 8, and lead 9. Neutrons are decelerated and then absorbed in the (up to 50 cm thick) paraffin and cadmium layers in the Cd(n,γ) reaction. The (up to 30 cm thick) lead layer absorbs photons. The shielding surrounding the detector contains a collimator defining the direction to the studied target 10.

The main sources of background are the Compton scattering of the bremsstrahlung radiation and e^+e^- pair production in the target studied. The last process leads to intense annihilation radiation with energy 0.511 MeV. To improve the background conditions, the detector as a rule is located at an angle θ larger than 90° relative to the direction of the bremsstrahlung radiation (usually, $\theta = 120$–$150°$). This leads, first, to a decrease in the number of γ quanta scattered on the detector side and, second, to a decrease of their average energy. The energy spectrum of the background radiation has a maximum in the range 300–600 keV. Since γ quanta with energies above 1–2 MeV are recorded in most $(\gamma,x\gamma')$ experiments, the signal-to-background ratio is improved by placing a lead filter 11 of thickness 2–4 cm between the target and the detector. To ensure that the detector is shielded from photoneutrons produced in the target, an additional shield made from a moderator (often paraffin up to 50 cm thick) and light matter which absorbs thermal neutrons (boron carbide, lithium fluoride, etc.) is often placed between the target and the detector.

The background is decreased further by recording γ quanta only at the moment of passage of the bremsstrahlung radiation. This makes it possible to eliminate the con-

TABLE I. Gamma lines used for energy calibration of the Ge(Li) spectrometer.

Radioactive isotope or reaction	Energy of the γ line, MeV
^{203}Hg	0,279
^{22}Na	0,511
^{137}Cs	0,662
^{60}Co	1,173 1,333
^{24}Na	1,368 2,754
^{208}Pb(n, $n'\gamma$)	2,615
^{27}Al(γ, $n\gamma'$)	4,71
^{16}O(γ, $n\gamma'$)	6,180 6,323
^{27}Al(p, γ)	10,761 12,073

tribution to the experimental spectrum from photons produced by the induced activity in the target matter and the surrounding materials. A plastic scintillation counter 12 located right by the accelerator is usually used for time selection of γ pulses recorded in the Ge(Li) detector. *In general, by these measures it is possible to decrease the background level by three to four orders of magnitude.*

The energy calibration of the γ spectrometer for $E_\gamma < 3$ MeV is done using standard radioactive sources with well known, strong γ lines. Their energies are given in Table I.

Gamma rays from nuclear reactions are used for the calibration in the region $E_\gamma > 2$ MeV. These reactions are also shown in Table I. Since the first reaction, ^{208}Pb(n,$n'\gamma$), is induced by photoneutrons produced by the bremsstrahlung radiation in the lead shielding, the corresponding background γ line is present in all experiments.

The reactions ^{16}O(γ,$n\gamma'$) and (γ,$p\gamma'$) are very convenient for calibration and development of the technique because distinct γ lines with energies 6.18 and 6.32 MeV are observed in them (see Fig. 5).

The gamma lines discovered in studying the reaction ^{16}O(γ,$x\gamma'$) using a Ge(Li) detector of sensitive volume 100 cm^3 (Ref. 12) are given in Table II. The same γ lines have been observed in other studies. They arise from γ transitions generated in the interaction of photoneutrons produced in the target with nuclei of the shielding and the Ge(Li) detector material. These γ lines cannot be eliminated by the background-reduction measures described above. These background γ lines will therefore be present also in the γ spectra from other targets. Their contribution must be taken into consideration in processing the experimental γ spectra.

To determine the partial cross sections for nuclear photodisintegration in (γ,$x\gamma'$) experiments, the peaks in the γ spectrum are identified with γ transitions between final-nucleus states. The states of the final nuclei populated in the photodisintegration of the nucleus under study are thereby uniquely determined. The shape of each peak is approximated by a smooth curve. The regions between the peaks are also approximated by smooth curves. The curves are drawn so as to give the best description of the experimental data. The background below each peak is determined by extrapolating the curves describing the photon spectrum in the energy range between the peaks to the region under the peaks. The area under the peak obtained after subtracting the background gives the number of re-

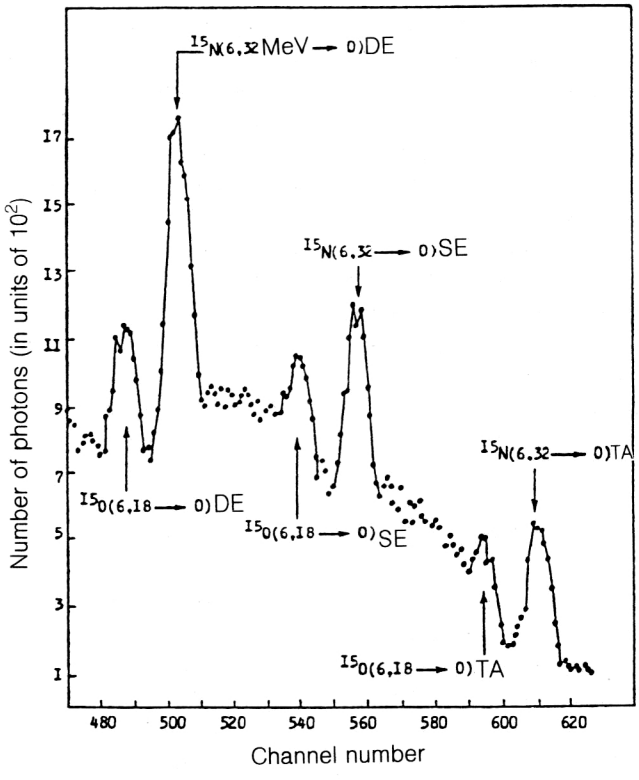

FIG. 5. High-energy part of the γ spectrum from the ^{16}O(γ,$x\gamma'$) experiment using a Ge(Li) detector of volume 100 cm^3 (Ref. 12).

TABLE II. Background γ lines from photoneutrons for the reaction $^{16}O(\gamma,x\gamma')$.

Energy of the γ line, MeV	Reaction
0,596	$^{74}Ge(n, n'\gamma) + {}^{72}Ge(n, n'\gamma)$
0,691	$^{72}Ge(n, n'\gamma)$
0,803	$^{206}Pb(n, n'\gamma)$
0,834	$^{72}Ge(n, n'\gamma)$
0,842	$^{27}Al(n, n'\gamma)$
0,897	$^{207}Pb(n, n'\gamma)$
1,013	$^{27}Al(n, n'\gamma)$
1,041	$^{70}Ge(n, n'\gamma)$
2,615	$^{208}Pb(n, n'\gamma)$

corded photons corresponding to a transition between the fth and ith states of the final nuclei (see Fig. 1). We shall call this number $N_{fi}(E^m)$, where E^m is the upper limit of the energy spectrum of the bremsstrahlung radiation incident on the target.

Next, the peaks are identified (it is determined whether they belong to TA, DE, or SE peaks) and the origin of the γ transitions is figured out. This is done using the known level schemes like those given in Ref. 13.

As an example, in Fig. 6 we show the spectrum of photons from a ^{27}Al target obtained by bombarding it with a bremsstrahlung γ beam with upper limit $E^m=32$ MeV (Ref. 14). The γ transitions between levels of the final nuclei ^{26}Mg and ^{26}Al contributing to each γ line of the spectrum are given, together with the processes occurring in the detector and leading to the detection of the corresponding γ quanta.

To calculate the partial photodisintegration cross section related to the population of the state f of the final nucleus, it is necessary to use the data on the number of γ transitions between final-nucleus states $N_{fi}(E^m)$ to calculate the number of DGR decays of the nucleus under study to the state f of the final nucleus recorded by the detector. We shall refer to this quantity as the f-line yield and denote it by $N_f(E^m)$. The given state f of the final nucleus can be populated both by direct decays into it of the DGR of the nucleus under study, and by a cascade of γ quanta leading to the population of the same state of the final nucleus (see Fig. 1). The state f itself can decay via the emission of γ quanta of various energies. Therefore, the number of recorded γ decays $N_{fi}(E^m)$ is related to the fth γ-line yield $N_f(E^m)$ as

$$\frac{1}{w_{fj}}N_{fj}(E^m)=\sum_{k>f}N_{kf}(E^m)+N_f(E^m), \tag{1}$$

where w_{fj} is the γ-decay probability of the state f with population of the state j. The quantity $\Sigma_{k>f}N_{kf}(E^m)$ is the recorded number of decays of kth states having excitation energy greater than that of the state f; the summation runs over all states k whose population is found by analyzing the photon spectrum. The values of w_{fj} in (1) are determined from the tabulated data on γ decays of nuclear states located below the nucleon-separation threshold. The values of $N_{kf}(E^m)$ are determined from the area under the corresponding γ peaks. By solving Eq. (1) we can determine the yield of the fth γ line. Computer processing of the experimentally measured γ spectra is widely used to determine the γ-line yields.[15]

The γ-line yields $N_f(E^m)$ obtained after preliminary processing of the photon spectrum are the initial information for finding the partial nuclear-photodisintegration cross sections. The γ-line yields $N_f(E^m)$ are related to the yields of photonuclear reactions leading to the population of the fth excited states of the final nuclei, $Y_f(E^m)$, as

$$Y_f(E^m)=\frac{N_f(E^m)}{vn\alpha\varepsilon\Omega\kappa(E^m)}, \tag{2}$$

where n is the number of bombarded target nuclei, ε is the γ detection efficiency, α is the attenuation coefficient for γ lines in the material between the target and the detector, Ω is the solid angle subtended by the detector, v is the density of the bremsstrahlung photon flux, and $\kappa(E^m)$ is the coefficient taking into account absorption in the target of bremsstrahlung radiation with upper limit E^m and photons of the γ line studied. The yields and partial nuclear-photodisintegration cross sections are related by an integral equation which is well known in the physics of photonuclear reactions:

$$Y_f(E^m)=\int_B^{E^m}\sigma_f(E)W(E,E^m)dE, \tag{3}$$

where B is the reaction threshold and $W(E,E^m)$ is the Schiff spectrum, normalized to the bremsstrahlung-photon flux density. Therefore, by measuring the spectra of scattered photons at different E^m and finding the γ-line yields $N_f(E^m)$, using (2) it is possible to calculate the reaction yield $Y_f(E^m)$. The partial cross sections $\sigma_f(E)$ are calculated by solving Eq. (3). This requires data on the density of the γ flux hitting the target.

The γ flux can be found by monitoring the beam with a perfect thick-walled ionization chamber. This method of measuring the partial cross sections is termed the *absolute* method. When the beam passes through a thick-walled chamber–monitor, both the absolute value of the γ flux and the shape of the bremsstrahlung spectrum are measured.

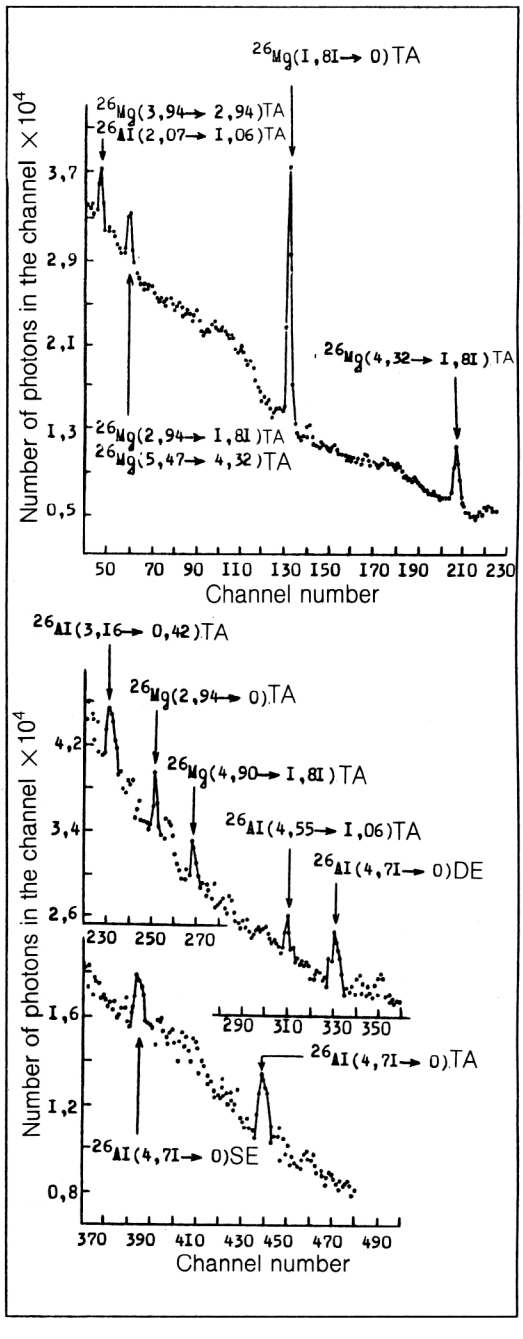

FIG. 6. Photon spectrum from the reaction ^{27}Al$(\gamma,x\gamma')$ obtained using a bremsstrahlung beam with upper limit 32 MeV and a Ge(Li) detector of volume 100 cm^3 (Ref. 14).

The inclusion of effects due to transformation of the photon beam necessary for finding $\sigma_f(E)$ in the absolute method is a very complex problem. Owing to these difficulties, *relative* methods have become widely used, along with the absolute method, for finding the partial cross sections in $(\gamma,x\gamma')$ experiments.

In relative methods the γ-line yields for the partial cross sections studied are compared with the yields of γ lines coming from deexcitation of levels, the partial cross sections for whose population are known from other experiments (henceforth such cross sections will be termed the *basis* cross sections). The yield of the reaction under study, $Y_f(E^m)$, is related to the yield $Y_r(E^m)$ calculated from the basis partial cross section as

$$Y_f(E^m)=\frac{N_f(E^m)\nu_r n_r \alpha_r \varepsilon_r \kappa_r(E^m)}{N_r(E^m)\nu n \alpha \varepsilon \kappa(E^m)}\,Y_r(E^m). \tag{4}$$

The subscript r denotes quantities determining the basis cross sections. After measuring the γ-line yields for the reaction channels under study, $N_f(E^m)$, and for the basis reaction, $N_r(E^m)$, using (4) to find the reaction yields $Y_f(E^m)$, and solving the inverse problem (3), the desired partial cross sections can be extracted. Relative methods are most effective when the cross sections under study and the basis cross sections for photodisintegration are measured simultaneously. In this case $\nu=\nu_r$ and Eq. (4) takes the simplest form:

$$Y_f(E^m)=\frac{N_f(E^m) n_r \alpha_r \varepsilon_r \kappa_r(E^m)}{N_r(E^m) n \alpha \varepsilon \kappa(E^m)}\,Y_r(E^m). \tag{5}$$

It follows from (5) that in determining the yields of the reactions under study it is no longer necessary to monitor the γ beam. It thereby becomes possible to eliminate the systematic uncertainties introduced during the beam monitoring in the absolute method. The partial cross section of the reaction ^{16}O(γ,p_3) populating the 6.32-MeV level of ^{15}N is often used as the basis cross section. This partial channel is characterized by a sizable integrated cross section amounting to 22.3 MeV · mb (for $E^m=30$ MeV), as a consequence of which the peak corresponding to population of the 6.32-MeV level of ^{15}N clearly stands out in the scattered γ spectrum (Fig. 5). The cross section for the reaction ^{16}O(γ,p_3) has been measured accurately in Ref. 16. The wide use of the partial cross section for photodisintegration of oxygen as the basis cross section is also due to the simplicity of preparing an oxygen target. Ordinary water can be used for it.

Methods of finding the partial photodisintegration cross sections using the photon spectra measured in $(\gamma,x\gamma')$ experiments have been studied in detail in Ref. 17. Analysis of all these methods leads to the following conclusions:

1. The systematic errors in determining the reaction yields for all methods are about the same and are $\approx$20–30%.

2. Each method has particular advantages and disadvantages, so that the decision to use a particular one must be made by taking into account the experimental goals.

3. All the methods give only the most general features of the energy distribution of the partial cross sections: the location of the center of gravity and the width. It is usually impossible to identify the intermediate structure of the partial cross sections in $(\gamma,x\gamma')$ experiments.

In many cases the γ-line yields are so small that they can be measured only for one or two upper limits of the bremsstrahlung-radiation spectrum. In this situation it is possible to find only the integrated partial cross sections, i.e., the cross sections integrated from threshold to the upper limit E^m of the bremsstrahlung spectrum. As a rule, the integrated cross sections can also be determined by a

relative method. The γ-line yield for the cross section under study is compared with the γ-line yield for the basis cross section measured at the same E^m. It is assumed that the *energy dependence of the cross sections is similar* for the basis reaction and the reaction under study, and the distortions related to the thresholds of these reactions are neglected. With these assumptions the ratio of the yields of the studied reaction and the basis reaction is equal to the ratio of their integrated cross sections, and the integrated cross section of the reaction under study, $\sigma_f^{\text{int}}(E^m)$, can be determined from the relation

$$\sigma_f^{\text{int}}(E^m)=\frac{Y_f(E^m)}{Y_r(E^m)}\,\sigma_r^{\text{int}}(E^m). \qquad (6)$$

In Refs. 17 and 18 methods are described which significantly decrease the systematic errors in finding the integrated partial cross sections due to the assumptions that the energy dependences of the cross sections of the studied and basis reactions are similar and that the difference of their thresholds insignificantly affects the accuracy of the final result.

To conclude this section, we note that the quantities $\sigma_f^{\text{int}}(E^m)$ given in the tables below for (γ,p) and (γ,n) reactions are, as a rule, obtained by multiplying by 4π the values of $d\sigma_f^{\text{int}}(\Theta)/d\Omega$ given by the authors for a single photon-detection angle Θ; in most cases $\Theta=140°$.

3. COMPARISON OF THE EXPERIMENTAL DATA FROM PARTICLE SPECTROMETRY AND FROM MEASUREMENT OF γ DEEXCITATION

Let us try to answer the question of what is the reliability of $(\gamma,x\gamma')$ experiments. This question often arises because, as seen from the preceding section, the analysis of the results of $(\gamma,x\gamma')$ experiments is a multistage, complex process. Of course, the authors of each experiment give the errors. The most convincing argument in favor of the reliability of the data is the fact that the results of independent experiments carried out in different laboratories agree. The results of both $(\gamma,x\gamma')$ experiments obtained by different groups and $(\gamma,x\gamma')$ experiments and experiments on the direct spectrometry of the x particle can be compared. In the range of mass numbers studied ($16<A\leqslant 40$) such comparisons can be made for several partial cross sections of the ^{23}Na, ^{24}Mg, ^{27}Al, ^{28}Si, ^{31}P, ^{32}S, and ^{40}Ca nuclei, for which independent experiments of both types have been carried out. As an example, in Table III we give the data on the *integrated* partial photonucleon cross sections for ^{40}Ca obtained in two $(\gamma,x\gamma')$ experiments[7,19] and one experiment on photoproton spectrometry.[19] We see that the data of the two $(\gamma,x\gamma')$ experiments agree within the errors quoted by the authors. It is true that a slightly larger number of partial channels were observed in the experiment of Ref. 7. However, all these channels have relatively small cross sections and mainly pertain to high-energy levels of the final nuclei ^{39}K and ^{39}Ca. Their observation in the experiment of Ref. 7 can be attributed to the use of a Ge(Li) detector with considerably larger sensitive volume (100 cm^3) compared with the 27-cm^3 Ge(Li) detector used in Ref. 19. On the whole, the results obtained by direct measurement of secondary γ quanta and by spectrometry agree. Of course, in the latter case the experimental data pertain to the sum of transitions to a large number of levels.

The dependence on the incident-photon energy was also obtained in Ref. 19 for several partial cross sections in the $(\gamma,x\gamma')$ experiment on ^{40}Ca. For this, the experiment was performed for 12 values of E^m (from 14 to 31 MeV). The data obtained are shown in Figs. 7a–7d. We see that the $(\gamma,x\gamma')$ experiment gives only a rough idea of the energy dependence of the partial cross sections when compared with the proton-spectrometry experiment carried out in the same study (see Figs. 7e and 7f). However, in the last experiment it is not possible to distinguish transitions to levels of the final nucleus ^{39}K with energies $E_f>2.8$ MeV. Let us consider the region $E_f=2.8$–4.2 MeV (the corresponding cross section is shown in Fig. 7f). In this energy range the ^{39}K nucleus has 10 levels. The $(\gamma,x\gamma')$ experiment of Ref. 19 shows that the cross section given in Fig. 7f is mainly produced by the population of three levels of the ^{39}K nucleus—the second and third excited states with energies 2.81 and 3.02 MeV and the sixth excited state with energy 3.94 MeV. It is these which are shown in Figs. 7b, 7c, and 7d. Another three levels (at 3.60, 3.88, and 4.08 MeV) are populated with considerably smaller probability. The energy dependences of the individual partial cross sections for the group of closely spaced adjacent levels of the final nucleus are also similar. Analogous data for other nuclei also indicate approximate similarity of the energy dependences of the partial cross sections for the population of closely spaced adjacent levels of the final nucleus. Therefore, the combined use of experimental data from γ and particle spectrometry makes it possible to determine fairly accurately the form of the partial cross sections from particle-spectrometry experiments and to determine which of the closely spaced levels of the final nucleus are populated and what their population probabilities are from decay-γ spectrometry experiments. Therefore, the results of these two types of experiment supplement each other.

It should be specially emphasized that experiments of these two types in this case give close values of the integrated cross sections for the population of low-lying levels of the ^{39}K nucleus in the reaction ^{40}Ca$(\gamma,p)^{39}$K (see Table III). For example, for the levels of the ^{39}K nucleus in the range 2.8–4.2 MeV, the $(\gamma,p\gamma')$ experiments of Refs. 19 and 7 give total integrated cross sections of 57 ± 5 and 51 ± 3 MeV · mb, respectively, while the (γ,p) experiment gives 50 ± 5 MeV · mb. Taking into consideration the difference in the upper limit of integration of the cross sections, the values of the integrated cross section for (γ,p_1) reactions obtained in these two types of experiment agree.

For the group of levels of the ^{39}K nucleus in the energy range 4.2–6.5 MeV the proton-spectrometry experiment of Ref. 19 gives the total integrated cross section 67 ± 8 MeV · mb (see Table III). The $(\gamma,p\gamma')$ experiment shows that in this energy range for ^{39}K, 7–10 levels are populated with total integrated cross section 42 ± 5 MeV · mb, which is 1.5 times lower than the value obtained by proton de-

TABLE III. Partial cross sections of the reactions $^{40}Ca(\gamma,p)^{39}K$ and $^{40}Ca(\gamma,n)^{39}Ca$ (Refs. 7 and 19) and characteristics of populated states of the final nuclei (Refs. 13 and 20).

Characteristics of levels of ^{39}K and ^{39}Ca						$\sigma^{int}(\gamma, p_f)$, $\sigma^{int}(\gamma, n_f)$, MeV · mb		
Order number f of the level of the final nucleus $A-1$	Final nucleus	Energy E_f of the level of the final nucleus, MeV	Spin and parity of the level, J^π	Hole structure of the level nl_j	Spectroscopic factor of the level C^2S^-	$(\gamma, x\gamma')$ [7] E^m = 32 MeV	$(\gamma, x\gamma')$ [19] E^m=30,25 MeV	(γ, p_f) [19] E^m=24,6 MeV
0	K	0	$3/2^+$	$1d_{3/2}$	3,97	110–120 оценки		100±7
	Ca				5,4	40–50 оценки		38±4 [21]
1	K	2,52	$1/2^+$	$2s_{1/2}$	1,65	61±2,1	59±4	49±5
	Ca	2,47			2,1	18,2±3,1	18±2	
2	K	2,81	$7/2^-$	$1f_{7/2}$	0,53	18,5±3,4	17±2	
	Ca	2,80			0,44		3±2	
3	K	3,02	$3/2^-$	$2p_{3/2}$	0,05	16,5±1,8	15±2	
	Ca	3,03			0,03			
4	K	3,60	$9/2^-$			3,6±1,7	2,3±1	
5	K	3,88	$3/2^-$	$2p_{3/2}$	0,02	3,4±1,4	2,9±0,7	
6	Ca	3,87	$(3/2^+)$					
	K	3,94	$3/2^+$			11±1,3	10,2±0,7	50±5
8	Ca	3,94	$(3/2^-)$	$(2p_{3/2})$	0,04			
	K	4,08	$3/2^-$	$(2p_{3/2})$		3,8±2,5	3,5±0,7	
10	Ca	4,02	$1/2^+$	$2s_{1/2}$	0,09	4,2±2,4		
13	Ca	4,49	$(5/2^+)$	$(1d_{5/2})$	0,1	1,7±0,9		
15	K	4,74	$(3/2^-—7/2^+)$			3,8±1,8		
16	K	4,93	$3/2^+$			6,3±1,8	5,4±0,8	
22	K	5,26	$5/2^+$	$1d_{5/2}$	1,0	6,4±1,5	6,5±1	
18	Ca	5,13			1,3	0,9±0,9	2,0±0,7	
21	K	5,17	$(1/2—7/2^+)$			1,3±0,8		
23	K	5,32	$3/2^+$			4,0±1,1	3,8±1,6	

TABLE III. (continued)

Characteristics of levels of ^{39}K and ^{39}Ca						$\sigma^{int}(\gamma, p_f)$, $\sigma^{int}(\gamma, n_f)$, MeV · mb		
Order number f of the level of the final nucleus $A-1$	Final nucleus	Energy E_f of the level of the final nucleus, MeV	Spin and parity of the level, J^π	Hole structure of the level nl_j	Spectroscopic factor of the level C^2S^-	$(\gamma, x\gamma')$ [7] E^m = 32 MeV	$(\gamma, x\gamma')$ [19] E^m=30,25 MeV	(γ, p_f) [19] E^m=24,6 MeV
26	K	5,60	$5/2^+$	$1d_{5/2}$	0,66	8,2±1,8	8±1	67±8
19	Ca	5,49			0,52	2,4±0,8	2,2±0,8	
28	K	5,71	$3/2^+$			1,8±0,9		
32	K	5,83	$(1/2, 3/2)^-$	$(2p_{3/2})$	0,05	2,6±1,5	2±1	
34	K	5,94	$(1/2, 3/2)^-$	$(2p_{3/2})$	0,03		1±1	
21	Ca	6,00	$(3/2)^-$		(0,02)	1,0±0,6		
42	K	6,35	$5/2^+$	$(1d_{5/2})$	1,25	6,7±1,4	7±1	
22	Ca	6,15	$(3/2, 5/2)^+$		1,3	1,1±0,6	1,5±0,8	
—	Ca	6,40	$(5/2^+)$	$(1d_{5/2})$	(0,25)	1,4±0,5		
49	K	6,55	$7/2^-$; T=3/2			2±1		
—	K	6,77	$(5/2^+)$	$(1d_{5/2})$	(0,1)	4±1,5		
—	Ca	6,92	$(5/2^+)$	$(1d_{5/2})$	(0,09)	3,7±1,3		
—	Ca	7,70	$(5/2^+)$	$(1d_{5/2})$	(0,1)	1,5±0,9		97±15
—								
—								
—	K	8,5						

Note: Populated mirror levels are located in successive rows. They are joined by a square bracket in the second column. The information about the hole structure of the levels is taken from Refs. 13 and 20.

tection. A similar situation also occurs for other nuclei. As the energy E_f of the final nucleus increases, the cross sections obtained from the particle-spectrometry experiment become larger and larger, exceeding the cross sections obtained in photon-spectrometry experiments. The systematic underestimate of the cross sections for large E_f in experiments of the latter type can be attributed to two factors. First, as E_f increases, more and more levels in a given energy range are populated, and the total cross section is split up more and more among many low-intensity transitions (see Table III). Since the sensitivity of Ge(Li) detectors to the photon energies decreases, part of the γ transitions of lowest intensity is not distinguished, and if there are enough of these, the total shortfall in the cross

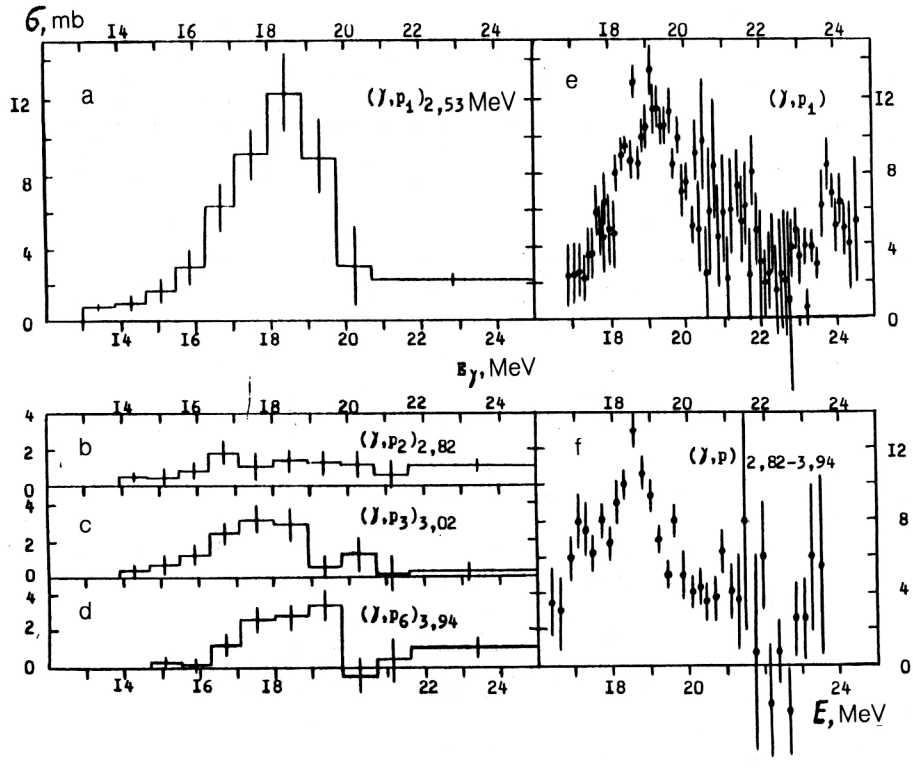

FIG. 7. Partial photoproton cross sections for ^{40}Ca obtained in Ref. 19 by spectrometry of the photons deexciting the final nucleus ^{39}K (a–d) and by proton spectrometry (e,f). The energies of the populated levels are given.

section can be large. Second, as E_f increases it becomes more difficult to disentangle the γ cascades, which can also lead to a loss of part of the cross section.

For levels of ^{39}K with $E_f = 6.5$–8.5 MeV the total value of the integrated cross section of the reaction ^{40}Ca(γ,p) observed in γ transitions is only 6 ± 2 MeV · mb. It follows from the proton-spectrometry experiment that the integrated cross section for the photoproton reaction in this range is 97 ± 15 MeV · mb. This large difference is only partially explained by the fact that the levels of ^{39}K in the range 6.5–8.5 MeV are unbound and decay only via proton emission (the proton separation energy for ^{39}K is 6.374 MeV). The cross section for the photoproton reaction in this range of E_f is the sum of $\sigma(\gamma,p)$ and $\sigma(\gamma,2p)$, and the integrated value of the latter in the range $E_\gamma < 24.6$ MeV is apparently less than 10 MeV · mb, according to the data of Ref. 7. Therefore, even in the most complete $(\gamma,p\gamma')$ experiment[7] in the range $E_f > 6.4$ MeV, the total value of the undefined (γ,p) cross section is $\gtrsim 80$ MeV · mb (it should be recalled that $E_\gamma \leqslant 32$ MeV in Ref. 7).

For the example of the reaction ^{40}Ca$(\gamma,p)^{39}$K just discussed, we have demonstrated the main features of, and differences between, the results of two types of experiment to determine the partial photonuclear cross sections. Before summarizing, let us give two more examples where results are compared.

In Fig. 8 we show the cross sections for the reaction ^{23}Na$(\gamma,p_1)^{22}$Ne obtained in Ref. 22 (γ spectrometry) and Ref. 23 (proton spectrometry). In Fig. 9 we compare the partial cross sections for the reaction ^{32}S$(\gamma,p)^{31}$P obtained in Ref. 24 (γ spectrometry) and Ref. 25 (proton spectrometry).

From these examples we arrive at the same conclusions as in the case of ^{40}Ca:

1. For low-lying levels of the final nucleus ($E_f \lesssim 4$ MeV) the values obtained for the cross sections and their approximate energy behavior in the two types of experiment are nearly the same.

2. As E_f grows ($E_f > 4$ MeV) the value of the cross section measured in γ-spectrometry experiments is under-

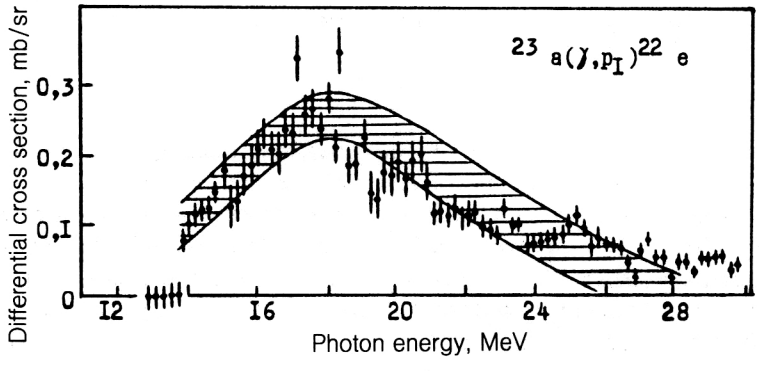

FIG. 8. Comparison of the cross sections for the reaction ^{23}Na$(\gamma,p_1)^{22}$Ne obtained by photon spectrometry[22] (shaded region) and proton spectrometry[23] (points).

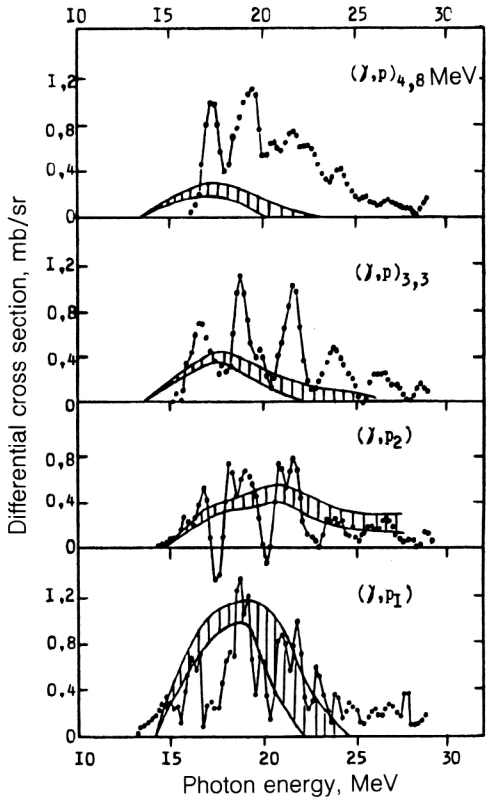

FIG. 9. Comparison of the partial photoproton cross sections for ^{32}S, obtained by photon[24] (shaded region) and proton[25] (points) spectrometry.

estimated more and more, and the form of the cross section becomes increasingly distorted. The degree of distortion grows with increasing level density.

3. The rough estimates of the energy dependences of the partial cross sections for closely spaced adjacent levels of the final nucleus are similar.

It follows that it is advisable to supplement the data from γ-spectrometry experiments by data from particle-spectrometry experiments. The cross sections and their energy dependences are determined more accurately in the latter. In the region of E_f where transitions to individual levels of the final nucleus overlap in particle-spectrometry experiments, these transitions can be distinguished in a γ-spectrometry experiment. Here the cross section for the population of a group of closely spaced levels of the final nucleus obtained in the particle-spectrometry experiment can be separated into the cross sections for the population of the individual levels-assuming that the partial cross sections for adjacent levels are roughly similar in form.

There are not yet many $(\gamma,x\gamma')$ experiments in which the energy dependences of the partial cross sections are obtained. For nuclei with $16 < A \leqslant 40$ there are four studies. The nuclei studied are ^{19}F (Ref. 26), ^{23}Na (Ref. 22), ^{32}S (Ref. 24), and ^{40}Ca (Ref. 19).

It follows from the above discussion that the difficulties of such experiments are primarily related to the complicated background conditions of $(\gamma,x\gamma')$ experiments and the low rate of statistics collection. Meanwhile, to obtain the energy dependence of the partial cross sections it is necessary to measure the yield $Y_f(E^m)$, varying E^m with a step of typically no more than 1.0–1.5 MeV. In such cases the method of information accumulation with fast scanning of E^m is quite effective in experiments at betatrons and synchrotrons. In this method, which has been used earlier in experiments to determine $\sigma(\gamma,p_f)$ by proton spectrometry (see Ref. 27, for example), E^m is changed in each electron acceleration event (i.e., with a typical frequency of 50 Hz), so that in a fraction of a second the entire set of chosen values is run through cyclically (or randomly). The memory of a multichannel pulse amplitude analyzer is divided into several segments corresponding to the different values of E^m, and information about the recorded particle spectra pertaining to a given E^m is automatically stored in the corresponding part of the memory.

This technique allows a considerable improvement of the accuracy of determining the energy dependence of the cross sections. Unfortunately, this method has not become widespread in $(\gamma,x\gamma')$ experiments. It has been used in only one case[22] to measure the cross section for the reaction $^{23}Na(\gamma,p_1)^{22}Ne$ (the result is shown in Fig. 8). A

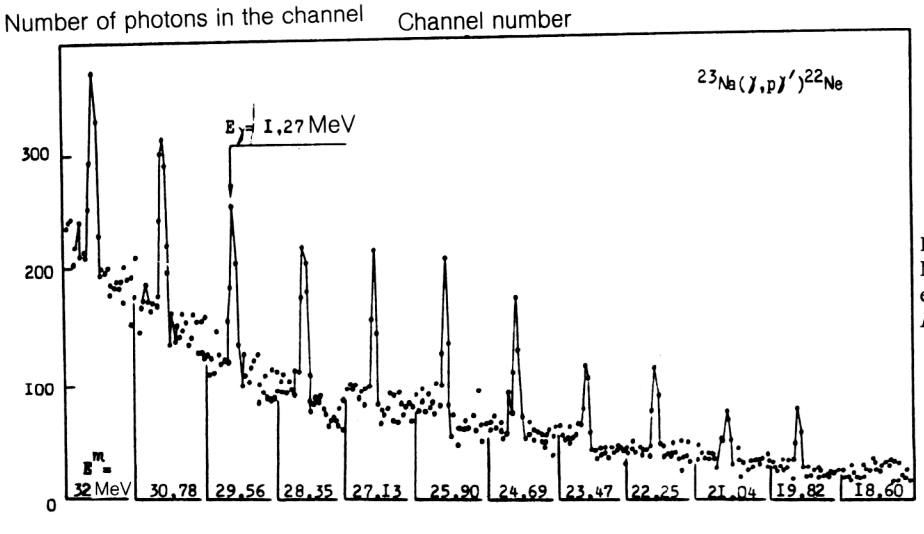

FIG. 10. Segments of the γ spectra near the 1.27-MeV line obtained in the $^{23}Na(\gamma,x\gamma')$ experiment[22] for various values of the upper limit E^m of the bremsstrahlung radiation.

TABLE IV. Summary of data on the partial photonuclear channels in $(\gamma,x\gamma')$ experiments (nuclei with $16<A\leqslant 40$)).

Target nucleus	Observed reactions	Highest energy of an observed populated level of the final nucleus, MeV	Highest energy of a photon of the bremsstrahlung radiation E^m, MeV	Experimental study
^{17}O	(γ, n), (γ, p)	6,13	28	[10]
^{18}O	(γ, n), (γ, p), $(\gamma, 2n)$, (γ, α)	6,73	28	[54]
^{19}F	(γ, n), (γ, p), (γ, α)	5,3	30	[26,55]
^{23}Na	(γ, n), (γ, p)	6,12	32	[5,22]
^{24}Mg	(γ, n), (γ, p), (γ, d), (γ, α)	6,0	30,5	[48,49]
^{25}Mg	(γ, n), (γ, p), (γ, d), (γ, α)	10,1	28,7	[49]
^{26}Mg	(γ, n), (γ, p), $(\gamma, 2n)$, (γ, α)	7,9	30	[49]
^{27}Al	(γ, n), (γ, p), (γ, np)	5,5	32	[14,50]
^{28}Si	(γ, n), (γ, p), (γ, α)	4,4	28	[32]
^{29}Si	(γ, n), (γ, p)	9,4	26	[6]
^{30}Si	(γ, n), (γ, p), $(\gamma, 2n)$, (γ, np), (γ, α)	8,3	26	[6]
^{31}P	(γ, n), (γ, p), (γ, np), (γ, α)	8,9	32	[8,55,56]
^{32}S	(γ, n), (γ, p), (γ, α)	7,2	32	[4,24,43]
^{39}K	(γ, n), (γ, p), (γ, α)	5,5	32	[9]
^{40}Ca	(γ, n), (γ, p), $(\gamma, 2p)$, (γ, τ), (γ, α)	7,7	32	[7,19]

detailed description of the technique for this experiment can be found in the dissertation of Gutiĭ.[22] It seems to us that this method has wider applicability. Here for illustration we shall restrict ourselves to the following information from Ref. 22. The energy of the first excited state of ^{22}Ne is 1.27 MeV. The quantity E^m ran through 16 values in the range 13–32 MeV, i.e., it was changed in steps of 1.2 MeV. A 4096-channel analyzer was used with its memory divided into 16 sections (each with 256 channels). Information on the spectrum of decay photons with energies in the range 0.3–3.0 MeV was stored in each. As an example, in Fig. 10 we show segments of the γ spectra near the 1.27-MeV line for 12 successive values of E^m (from 18.6 to 32 MeV) obtained in one series of measurements.

We conclude this section by giving Table IV, in which the data of $(\gamma,x\gamma')$ experiments carried out for nuclei in this region are summarized.

4. THE METHOD OF ISOLATING SEMIDIRECT NUCLEONS IN DGR DECAY

The partial cross section $\sigma^q(\gamma,x_f)$ of a semidirect photonucleon reaction ($x=p$ or n) occurring via an isolated resonance q due to the emission of a particle x and related to the population of the level f can be written as

$$\sigma^q(\gamma,x_f)=\sigma^q_\gamma\frac{\Gamma^\uparrow(x_f)}{\Gamma_q}. \tag{7}$$

Here σ^q_γ is the cross section for total γ absorption related to the excitation of this resonance; $\Gamma^\uparrow(x_f)$ is the resonance width related to the semidirect emission of a nucleon x and the population of the state f; Γ_q is the total resonance width, including the width related to the spread of the doorway states.

The ratio of the partial cross sections for processes occurring via the resonance q and due to a semidirect process is equal to the ratio of the widths $\Gamma^\uparrow(x_f)$:

$$\frac{\sigma^q(\gamma,x_1)}{\sigma^q(\gamma,x_2)}=\frac{\Gamma^\uparrow(x_1)}{\Gamma^\uparrow(x_2)}. \tag{8}$$

We can assume (the arguments will be presented at the end of this section) that the ground and lowest states of the final nucleus $(A-1)$, which have a hole nature, are populated as a result of a semidirect process. Taking the cross sections for the population of the ground and lowest-lying states from experiment and assuming that they have an exclusively semidirect nature, we can calculate the partial cross sections of the semidirect decay of this resonance into higher hole states. Of course, for this it is necessary to know the width ratio. An excess of the measured cross section $\sigma_{\rm exp}(\gamma,x_f)$ over the cross section calculated by this method, for example,

$$\sigma_{\rm th}(\gamma,x_f)=\sigma_{\rm exp}(\gamma,x_0)\frac{\Gamma^\uparrow(\gamma,x_f)}{\Gamma^\uparrow(\gamma,x_0)}, \tag{9}$$

will imply that the cross-section excess

$$\Delta=\sigma_{\rm exp}(\gamma,x_f)-\sigma_{\rm th}(\gamma,x_f)$$

is related to a preequilibrium or equilibrium process.

However, the ratio of the widths $\Gamma^{\uparrow}(x_f)$ is unknown. It must be calculated. This is most often done by using the traditional shell model, at first neglecting the fact that the resonance is located in the continuum. This is the bound shell model (BSM). To describe the decay of a resonance state, an interaction with the continuum is introduced on the basis of R-matrix theory, using the reduced-width formalism. In this case the partial width of an isolated resonance for the emission of a nucleon with the quantum numbers (n,l,j) and the formation of a final nucleus in the state $f(E,J,T)$ is described by the expression

$$\Gamma_{\lambda f}(q)=2\sqrt{\varepsilon_f}\gamma_0^2 P_{q\lambda}(\varepsilon_f)S_{\lambda}(q\to f). \tag{10}$$

Here ε_f is the energy of the emitted nucleon, $P_{q\lambda}(\varepsilon_f)$ is the penetration factor of the Coulomb and centrifugal barriers, γ_0^2 is the reduced spectroscopic factor, and $S_{\lambda}(q\to f)$ is the *spectroscopic factor relating an isolated resonance q to states of the final nucleus* $(A-1)$ *and the nucleon in the continuum with the quantum numbers* $\lambda=(l,j)$.

By now methods have been developed which allow the continuum to be taken into account directly in the construction of doorway states [the continuous shell model (CSM)]. It thereby becomes possible to avoid the inconsistencies of the combined BSM and R-matrix approach. However, the conceptual and technical difficulties which arise for this model mean that it is rarely used for analyzing experimental data. The BSM in combination with the R-matrix approach is attractive in that the formalism is easy (owing to some loss of rigor) to use for analyzing experimental data, at least for strong transitions (transitions to levels of the final nucleus with large spectroscopic factors).

It is natural to wonder how reliable the method is. We shall use one important result obtained in the CSM: for transitions with large spectroscopic factors, the partial width can be factorized in the form of a spectroscopic factor and a penetration factor—Eq. (10). Otherwise, the problem of obtaining the partial widths from the spectroscopic factors is nontrivial.[28] Secondly,[29] for transitions with large spectroscopic factors the ratios of the partial widths obtained in the CSM and the BSM with the R-matrix approach turn out to be close.

To calculate the partial widths using (10), it is necessary to know the wave function of the resonance state q. The isolated doorway states forming the bulk of the dipole resonance can be written as a superposition of states

$$|q\rangle=\sum_{\alpha>\beta}X_{\alpha\beta}(q)a_{\alpha}^{+}a_{\beta}\Psi_{gr}, \tag{11}$$

constructed above the physical ground state of the target nucleus, Ψ_{gr}. In Ψ_{gr} we shall neglect correlations of nucleons which take them out of the band of filled lowest shells. For nuclei in the region studied, the effect of these correlations in the ground state is 20–30% (Refs. 30 and 31). The corresponding correlations are, of course, also neglected in the resonance wave function. In Eq. (11), α and β are indices distinguishing the single-particle states (the inequality $\alpha>\beta$ means that the nucleon energy in the state α is higher than in the state β). Here a_{α}^{+} and a_{β} are the creation and annihilation operators of nucleons in the states α and β, respectively, and $X_{\alpha\beta}(q)$ are the amplitudes with which the components $a_{\alpha}^{+}a_{\beta}\Psi_{gr}$ enter the resonance wave function.

Now we restrict ourselves to only those *doorway states* in (11) *which are formed by transitions of nucleons from outer shells.* Then the spectroscopic factors $S_{\lambda}(q\to f)$ are proportional to the spectroscopic factor $S^{-}(f)$ of the reaction of nucleon capture from the ground state of the initial nucleus A and formation of the nucleus A–1 in the state f. Up to a constant the expression for the partial width of an even–even nucleus A has the form

$$\Gamma_{\beta}^{\uparrow}(q\to f)=\text{const}\,S_{\beta}^{-}(f)\sqrt{\varepsilon_f}\sum_{\alpha}P_{\alpha}(\varepsilon_f)X_{\alpha\beta}^{2}(q), \tag{12}$$

where the index $\beta=(n_{\beta},l_{\beta},j_{\beta},\pi_{\beta})$ indicates the type of hole excitation present in the final state f (i.e., it means that the nucleon was ejected from the single-particle state β upon absorption of a photon by the nucleus).

Since only doorway states are involved in the construction of the wave function, the calcuated width by definition corresponds to the semidirect nucleon-emission width. We see from the above expressions that this width is proportional to the spectroscopic factor appearing in the capture reaction. This proportionality (correlation) was noted in Refs. 24, 27, and 32–35. Equation (12) was obtained directly in Ref. 36.

For an odd nucleus the expression for the width of a semidirect process is somewhat complicated:[36]

$$\Gamma_{\beta}^{\uparrow}(q\to f)=\text{const}\,\frac{\sqrt{\varepsilon_f}}{N_{\beta}^{2}}(1/2\tau_x T_f T_0-\tau_x|T_q T_0)^2 \times\begin{Bmatrix}1/2 & 1/2 & 1\\ T_0 & T_q & T_f\end{Bmatrix}R_{\beta}(q)S_{\beta}^{-}(f) \times(2j_{\beta}+1)\sum_{\alpha}P_{\alpha}(\varepsilon_f)X_{\alpha\beta}^{2}(q), \tag{13}$$

where N_{β} is the number of nucleons in the subshell β in the ground state of the nucleus; $(....|..)$ are the Clebsch–Gordan coefficients; $\{\cdots\}$ are the Wigner symbols; τ_x is the isospin projection of the emitted nucleon ($\tau_x=1/2$ for the neutron and $-1/2$ for the proton); T_f is the isospin of the final state. The summation over α in (12) essentially reduces to summation over the orbital angular momentum l of the emitted nucleon. $R_{\beta}(q)$ has the form[36]

$$R_{\beta}(q)=\frac{(T_q+T_0+2)(T_0+1-T_q)}{4T_0}\nu_{\beta}(n) +\frac{(T_q+T_0)(T_q+1-T_0)-2}{4T_0}\nu_{\beta}(p), \tag{14}$$

where $\nu_{\beta}(n)$ and $\nu_{\beta}(p)$ are the neutron and proton populations of the subshell β [for example, $\nu_{\beta}(n)$ is equal to $n_{\beta}/(2j_{\beta}+1)$], which, like N_{β} and $S_{\beta}^{-}(f)$, are taken from the experimental data on one-nucleon transfer reactions.

Equation (13) contains the explicit isospin structure of the DGR states of an odd nucleus. We recall that for an

odd nucleus the spin and isospin of the ground state (J_0,T_0) are nonzero, while the spin and isospin of dipole states can take various values (three values for J: J_0, $J_0\pm1$; two values for T_q: T_0 and T_0+1).

In the case of an odd target nucleus, in the final (after nucleon emission) state f there can be more than one type of hole excitation β, in contrast to the version with an even–even target nucleus. In this case

$$\Gamma^{\uparrow}(q\to f)=\sum_{\beta}\Gamma^{\uparrow}_{\beta}(q\to f).$$

For an even–even target nucleus

$$\Gamma^{\uparrow}(q\to f)\equiv\Gamma^{\uparrow}_{\beta}(q\to f)\ \text{and}\ S^{-}_{\beta}(f)\equiv S^{-}(f).$$

For an even–even nucleus the ratio of the partial widths of a semidirect process is given by

$$\frac{\Gamma^{\uparrow}_{\beta_1}(q\to f_1)}{\Gamma^{\uparrow}_{\beta_2}(q\to f_2)}=\frac{S^{-}_{\beta_1}(\varepsilon_1)}{S^{-}_{\beta_2}(\varepsilon_2)}\sqrt{\frac{\varepsilon_1}{\varepsilon_2}}\frac{\Sigma_\alpha P_\alpha(\varepsilon_1)X^2_{\alpha\beta_1}(q)}{\Sigma_\alpha P_\alpha(\varepsilon_2)X^2_{\alpha\beta_2}(q)}. \qquad (15)$$

A similar relation can be written down also for an odd nucleus. To calculate the ratio (15) it is necessary to know the explicit structure of the wave function of the state $|q\rangle$, i.e., the coefficients $X_{\alpha\beta}$. However, let us consider limiting cases in order to obtain an idea of the range of variation of this ratio.

The quantities $\Gamma^{\uparrow}_{\beta}(q\to f)$ involve the sums $\Sigma_\alpha P_\alpha(\varepsilon_1)X^2_{\alpha\beta}(q)$. A dipole resonance of nuclei of the $1d2s$ shell coupled to nucleons of an outer shell is formed from $1d2s\to1f2p$ nucleon transitions:

$$d_{5/2}\to f_{7/2},f_{5/2},p_{3/2};$$

$$d_{3/2}\to f_{5/2},p_{3/2},p_{1/2};$$

$$s_{1/2}\to p_{3/2},p_{1/2}.$$

Therefore, semidirect nucleons leave either the p shell or the f shell, carrying orbital angular momentum $l=1$ or 3. The sum $\Sigma_\alpha P_\alpha X^2_{\alpha\beta}$ can be split into two terms corresponding to $l=1$ and 3:

$$\sum_{\alpha}P_\alpha X^2_{\alpha\beta}=P_1X^2_1+P_3X^2_3,$$

where

$$X^2_1=X^2_{d_{5/2}p_{3/2}}+X^2_{d_{3/2}p_{3/2}}+X^2_{d_{3/2}p_{1/2}}+X^2_{s_{1/2}p_{3/2}}+X^2_{s_{1/2}p_{1/2}},$$

$$X^2_3=X^2_{d_{5/2}f_{7/2}}+X^2_{d_{5/2}f_{5/2}}+X^2_{d_{3/2}f_{5/2}},$$

with $X^2_1+X^2_3=1$, and P_1 and P_3 are the barrier penetration factors for nucleons with $l=1$ and 3.

Let us compare the partial transitions to different levels of the same hole nature ($\beta_1=\beta_2$). There are two limiting cases, when nucleons with $l=1$ or $l=3$ are emitted from the nucleus. According to (15), the corresponding limiting ratios of the partial widths of semidirect decay are then given by

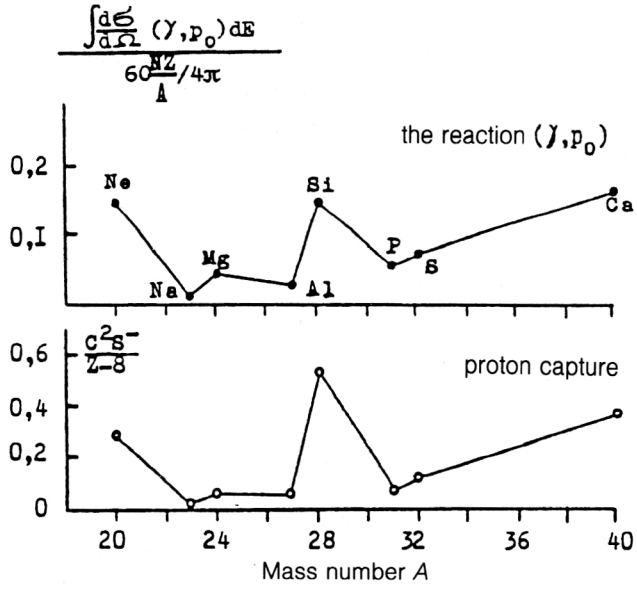

FIG. 11. Correlation between the values of the (γ,p_0) cross sections and the spectroscopic factors of the proton capture reaction for nuclei of the $1d2s$ shell (details in the text).

$$\frac{\Gamma^{\uparrow}(q\to f_1)}{\Gamma^{\uparrow}(q\to f_2)}=\begin{cases}\dfrac{S^{-}(\varepsilon_1)}{S^{-}(\varepsilon_2)}\sqrt{\dfrac{\varepsilon_1}{\varepsilon_2}}\dfrac{P_1(\varepsilon_1)}{P_1(\varepsilon_2)} & \text{for } l=1\\ \dfrac{S^{-}(\varepsilon_1)}{S^{-}(\varepsilon_2)}\sqrt{\dfrac{\varepsilon_1}{\varepsilon_2}}\dfrac{P_3(\varepsilon_1)}{P_3(\varepsilon_2)} & \text{for } l=3.\end{cases}$$

All the intermediate values of the ratio $\Gamma^{\uparrow}(q\to f_1)/\Gamma^{\uparrow}(q\to f_2)$ corresponding to different degrees of mixing of nucleons with $l=1$ and 3 will lie between the two limiting values calculated above. Therefore, in general (after the cancellation of common factors) we can write

$$\frac{P_1(\varepsilon_1)}{P_1(\varepsilon_2)}\leqslant\frac{\Gamma^{\uparrow}(q\to f_1)}{\Gamma^{\uparrow}(q\to f_2)}\leqslant\frac{P_3(\varepsilon_1)}{P_3(\varepsilon_2)}. \qquad (16)$$

We did not need the structure of the wave function to estimate this ratio. Let us give the value of the inequality for the ^{28}Si target nucleus and the photoneutron energies $\varepsilon_1=8$ MeV and $\varepsilon_2=4$ MeV:

$$1.2\leqslant\frac{\Gamma^{\uparrow}(q\to f_1)}{\Gamma^{\uparrow}(q\to f_2)}\leqslant4.0.$$

Equation (16) can be used to find the upper and lower limits on $\Gamma^{\uparrow}$ corresponding to the emission of a nucleon only with $l=1$ or $l=3$.

The approach described above has been used to isolate the semidirect DGR decay branch in Refs. 2, 27, 33, and 36. As noted above, for nuclei of the $1d2s$ shell it is assumed that the cross section for populating the ground state is related exclusively to the semidirect process. We shall refer to this as the *reference* cross section.

The partial (γ,p_0) cross section can be obtained accurately from the data on the inverse (p,γ_0) reaction, using the detailed-balance equation. These experiments are usually carried out with high (≈10 keV) energy resolution at electrostatic accelerators. Analysis of the Ericson fluctua-

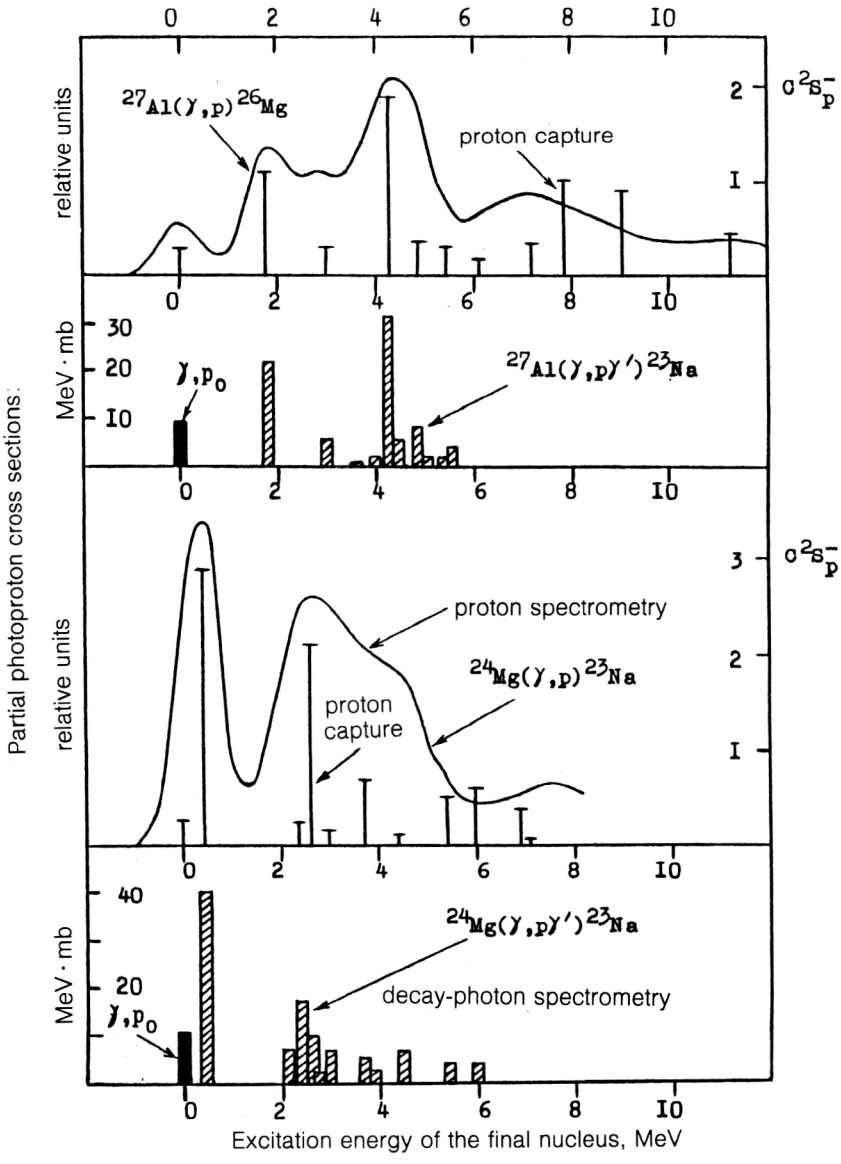

FIG. 12. Correlations between the partial photoproton cross sections and the spectroscopic factors of proton capture $C^2S_p^-$ (vertical lines) for ^{24}Mg and ^{27}Al. The partial photoproton cross sections were obtained by both photon (shaded columns) and proton (solid lines) spectrometry. The cross sections of the (γ,p_0) reaction were obtained from (p,γ_0) experiments.

tions observed in these cross sections showed[37–42] that they are dominated by direct (semidirect in our terminology) processes. For example, for ^{28}Si, ^{32}S, and ^{40}Ca the probability of semidirect decay in the (γ,p_0) channel is 0.87–0.99. This is indicated by the strong correlation between the spectroscopic factors S_0^- of the ground states of the final nuclei and the integrated values of the (γ,p_0) cross sections. The degree of this correlation is demonstrated in Fig. 11. In the upper part of the figure we show the integrated cross sections of the (γ,p_0) reaction relative to the classical dipole sum rule ($60NZ/A$ MeV · mb), and in the lower part we show $C^2S_0^-/(Z-8)$, where S_0^- is the spectroscopic factor of the ground state of the final nucleus, $C^2=2T_f/(2T_f+1)$, T_f is the isospin of the final state (in our case the ground state), and $(Z-8)$ is the number of protons outside the inert ^{16}O core.

A correlation with the data on capture reactions is also observed for the partial cross sections for the occupation of the very lowest excited states of the final nuclei, which, as a rule, have a hole nature. This is clearly seen from Fig. 12, where we compare the data on capture reactions[13,20] and on (γ,p_f) reactions for ^{24}Mg (Refs. 47–49) and ^{27}Al (Refs. 14 and 51). This indicates that semidirect decay dominates also in these partial cross sections, which for this reason can also be used as *reference* ones. A similar result was obtained in calculations of the partial nucleon- decay channels of DGR of ^{28}Si and ^{32}S carried out in Refs. 30, 44, and 45. The criterion (8) can also be used to select the partial photonucleon cross sections produced mainly owing to semidirect decay.

Equations (8), (9), and (12)–(16) formed the basis of a method for isolating the semidirect branch of giant dipole- resonance decay (Refs. 2, 27, 33, and 36).

5. ISOLATION OF THE SEMIDIRECT BRANCH OF DGR DECAY IN THE NUCLEI ^{24}Mg AND ^{27}Al

The energy dependences of the partial photoproton cross sections obtained in proton-spectrometry experiments are available for even–even self-conjugate nuclei (^{24}Mg, ^{28}Si, ^{32}S, and ^{40}Ca). These data are supplemented by the data of $(\gamma,x\gamma')$ experiments, obtained in most cases

for one or two values of the upper limit E^m of the bremsstrahlung radiation. We shall consider the analysis of this category of experimental data for the example of ^{24}Mg, following Ref. 46.

For the other group of nuclei, non-self-conjugate nuclei (see Table IV), only the results of $(\gamma,p\gamma')$ and $(\gamma,n\gamma')$ experiments on the integrated partial photonucleon cross sections can be analyzed. The data from particle-spectrometry experiments in this case are used only to monitor the correctness of the results of $(\gamma,x\gamma')$ experiments. The reason for this will become clear in the following discussion. As an example of analyzing this group of data, we shall describe the analysis of the results of the $(\gamma,x\gamma')$ experiment for ^{27}Al, following Ref. 36.

A complete analysis of the contribution of semidirect nucleons is possible only when both the partial photoproton cross sections and the partial photoneutron cross sections are known. The latter, as a rule, have not been measured. Only the total photoneutron cross sections $\sigma(\gamma,n)=\Sigma_f\sigma(\gamma,n_f)$ have been measured. However, in the case of even–even self-conjugate nuclei ($N=Z$), indirect information can be obtained[2,33] on the partial photoneutron cross sections by converting them from the partial photoproton cross sections, using several assumptions. Let us list these:

1. The isospin of low-lying states of the final nucleus ($T=1/2$) and the ground state of the initial nucleus ($T=0$) is a good quantum number.

2. The isospin of the dipole state that is formed ($T=1$) is also a good quantum number.

In this case, for an initial even–even self-conjugate nucleus, neglecting (1) the difference between the proton and neutron decay thresholds, (2) the slight difference in the energy position of the mirror levels of the final nuclei, and (3) the penetration factor of the Coulomb barrier, the cross section for the partial photoneutron channel must mimic that of the mirror photoproton channel. Actually, these factors must be taken into account, and the cross section must be converted.

The conversion procedure consists of the following. Each partial cross section $\sigma(\gamma,p_f)$ is converted, taking into account the information about the orbital angular momentum of the emitted nucleons in the corresponding cross section $\sigma(\gamma,n_f)$. This is done by using the relation

$$\frac{\sigma(\gamma,n_f)}{\sigma(\gamma,p_f)}=\sqrt{\frac{\varepsilon_n}{\varepsilon_p}}\frac{P_n(\varepsilon_n)}{P_p(\varepsilon_p)}, \tag{17}$$

where P_n and P_p are the barrier penetration factors for protons and neutrons, and ε_n and ε_p are their kinetic energies. Then the $\sigma(\gamma,n_f)$ thus obtained are summed and compared with the measured total cross sections $\sigma(\gamma,n)$. Good agreement in both the shape and the absolute value of the compared cross sections is possible only for an insignificant mixture of dipole states with $T=0$ in dipole states with $T=1$.

The photoproton partial cross sections have been converted to photoneutron ones for ^{12}C, ^{16}O, ^{40}Ca (Refs. 2 and 33), and ^{32}S (Refs. 12 and 43). Good agreement between the converted total photoneutron cross sections and the experimental ones is obtained, confirming the conclusion about the fairly high isospin purity of DGR states of light self-conjugate nuclei and the correctness of applying the conversion procedure $\sigma(\gamma,p_f)\rightarrow\sigma(\gamma,n_f)$ to these nuclei.

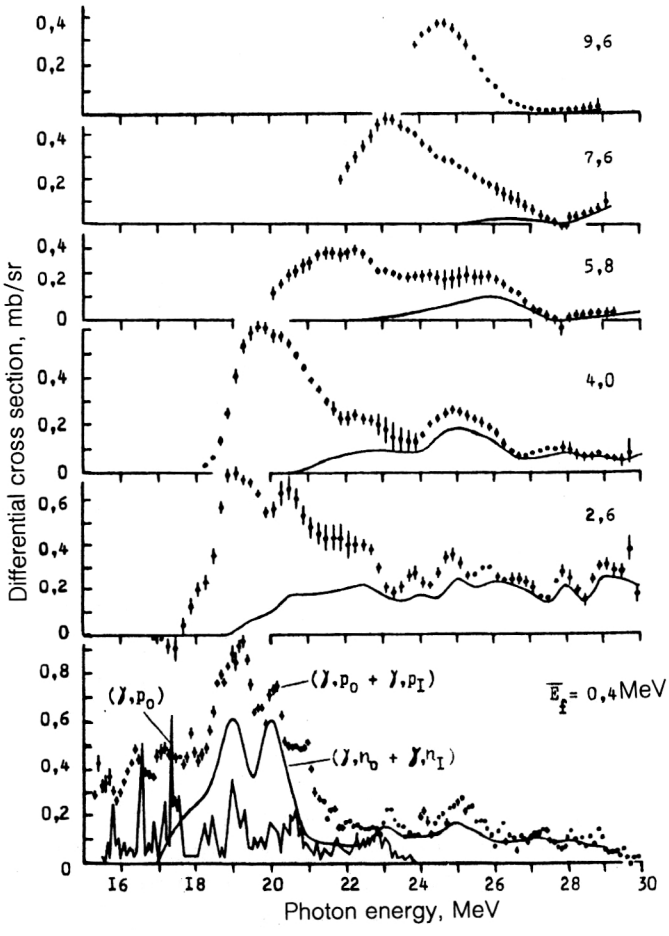

FIG. 13. Partial photoproton[47] (points) and photoneutron (solid lines) cross sections for ^{24}Mg. The centers of gravity of the populated groups of levels are given. In the lower figure we also give the cross section for the (γ,p_0) reaction from the (p,γ_0) experiment of Ref. 39.

The conversion results depend on the orbital angular momentum l of the emitted nucleon. In most cases l is unknown. Only a set of possible values can be given for it, using the angular-momentum and parity selection rules. In these cases the conversion $\sigma(\gamma,p_f)\rightarrow\sigma(\gamma,n_f)$ will be carried out for two values of l: the minimum ($l_{\min}$) and the maximum ($l_{\max}$).

The nucleus ^{24}Mg

The energy dependences of $\sigma(\gamma,p_f)$ for ^{24}Mg were obtained in Refs. 47 and 48. The rest of the analysis is based on the data of Ref. 47, shown in Fig. 13. These data contain information not only about the cross sections for the population of low-lying (<4 MeV) levels of the ^{23}Na nucleus, but also about the cross sections for the population of high-lying (up to 10 MeV) levels of the final nucleus. All the partial cross sections given in Ref. 47 are cross sections for the population of several (at least two) states of the final nucleus. The (γ,p) channels studied are listed

TABLE V. Mirror channels of DGR decay for ^{24}Mg.

Channels studied in Ref. 47	(γ, p_f)	(γ, n_f)	E_f, MeV ^{23}Na	E_f, MeV ^{23}Mg	J^π	Hole configurations nl_j	S_p^-	S_n^-	Nucleon orbital angular momentum l_{min}	l_{max}
$(\gamma, p)_{\bar{E}_f=0,4}$ MeV	γ, p_0	γ, n_0	0	0	$3/2^+$	$1d_{3/2}$	0,51	0,66	1	3
	γ, p_1	γ, n_1	0,44	0,45	$5/2^+$	$1d_{5/2}$	5,9	4,4	1	3
	γ, p_2	γ, n_2	2,08	2,05	$7/2^+$				3	
	γ, p_3	γ, n_3	2,39	2,36	$1/2^+$	$2s_{1/2}$	0,49	0,36	1	
$(\gamma, p)_{2,6}$	γ, p_4	γ, n_5	2,64	2,77	$1/2^-$	$1p_{1/2}$	4,2	4,6	0	2
	γ, p_5	γ, n_4	2,70	2,72	$9/2^+$				3	
	γ, p_6	γ, n_6	2,98	2,91	$3/2^+$	$1d_{3/2}$	0,32	0,28	1	3
	γ, p_7	γ, n_7	3,68	3,80	$3/2^-$	$1p_{3/2}$	1,4	0,72	0	2
$(\gamma, p)_{4,0}$	γ, p_8	γ, n_9	3,85	3,97	$5/2^-$				2	
	γ, p_9	γ, n_8	3,91	3,86	$5/2^+$	$1d_{5/2}$	0,03	0,03	1	3
	γ, p_{10}	γ, n_{10}	4,43	4,36	$1/2^+$	$2s_{1/2}$	0,18	0,11	1	
$(\gamma, p)_{5,8}$	γ, p_{12}	γ, n_{12}	5,38	5,29	$5/2^+$	$1d_{5/2}$	0,98	1,1 (?)	1	3
	γ, p_{18}	γ, n_{18}	5,97	5,99	$3/2^-$	$1p_{3/2}$	1,2	4,0 (?)	0	2
$(\gamma, p)_{7,6}$		$(\gamma, n)_{7,6}$	6,5—8,5			$1p_{3/2}$	0,9		0	3
$(\gamma, p)_{9,6}$		$(\gamma, n)_{9,6}$	8,5—10,5			$1p_{3/2}$	1,2—2,4		0	3

in the left-hand column of Table V. The centers of gravity $\bar{E}_f$ of the populated groups of levels are given. The division of these cross sections into the cross sections for the population of individual levels of ^{23}Na was done using $\sigma(\gamma,p_0)$ taken from the (p,γ_0) experiment of Ref. 39, and the data of $(\gamma,p\gamma')$ experiments[48,49] (Table VI). Experiments of the latter type, in which the integrated partial cross sections are determined for individual levels, showed that the cross sections for the population of groups of levels of ^{23}Na with $\bar{E}_f$=2.6, 4.0, and 5.8 MeV are formed owing to the tran-

TABLE VI. Integrated cross sections of ^{24}Mg$(\gamma,p_f)^{23}$Na reactions and characteristics of populated levels of ^{23}Na (Refs. 13 and 20).

Level characteristic of ^{23}Na					$\sigma^{int}(\gamma, p_f)$, MeV · mb		
f	E_f, MeV	J^π	nl_j	C^2S^-	$\gamma, p\gamma'$ [49] E^m=30,5 MeV	$\gamma, p\gamma'$ [48] E^m=28,5 MeV	γ, p [47] E^m=30MeV
0*	0	$3/2^+$	$1d_{3/2}$	0,26	—	—	11
1*	0,44	$5/2^+$	$1d_{5/2}$	2,9	—	—	40
2	2,08	$7/2^+$			<8,90	<12,9±1,1	
3*	2,39	$1/2^+$	$2s_{1/2}$	0,24	10,56	16,8±1,3	
4*	2,64	$1/2^-$	$1p_{1/2}$	2,1	8,02	10,0±0,8	52
5	2,70	$9/2^+$			<2,80	<1,8±1,0	
6	2,98	$3/2^+$	$1d_{3/2}$	0,16	5,73	6,3±1,3	
7*	3,68	$3/2^-$	$1p_{3/2}$	0,7	4,44	5,2±1,2	
8	3,85	$5/2^-$			2,03	0	32
9	3,91	$5/2^+$	$1d_{5/2}$	0,015	6,27	1,9±0,8	
10	4,43	$1/2^+$	$2s_{1/2}$	0,09	6,53	6,1±0,6	
12	5,38	$5/2^+$	$1d_{5/2}$	0,49	1,89	3,8±1,5	18
18	5,97	$3/2^-$	$1p_{3/2}$	0,6	<3,5	4,3±1,6	
	6,5–8,5				—	—	18
	8,5–10,5				—	—	9

Levels whose population cross sections were used as the reference cross sections

TABLE VII. Integrated cross sections of $^{24}Mg(\gamma,n_f)^{23}Na$ reactions and characteristics of populated levels of ^{23}Mg (Refs. 13 and 20).

Level characteristics of ^{23}Mg					$\sigma^{int}(\gamma, n_f)$, MeV · mb		
f	E_f, MeV	J^π	nl_j	C^2S^-	$\gamma, n\gamma'$ [49] E^m=30,5 MeV	$\gamma, n\gamma'$ [48] E^m=28 MeV	Conversion from (γ,p_f) [46] E^m=30 MeV
0*	0	$3/2^+$	$1d_{3/2}$	0,33	—	—	6
1*	0,45	$5/2^+$	$1d_{5/2}$	2,2	—	—	24
2	2,05	$7/2^+$			0,85	2,6±1,0	5—6
3*	2,36	$1/2^+$	$2s_{1/2}$	0,18	2,13	3,4±1,0	12
4	2,72	$9/2^+$			<1,79	<1,7±1,0	1
5*	2,77	$1/2^-$	$1p_{1/2}$	2,3	3,05	2,5±0,4	5—6
6	2,91	$3/2^+$	$1d_{3/2}$	0,14	—	3,9±1,3	2—3
7*	3,80	$3/2^-$	$1p_{3/2}$	0,36	—	—	3—3,5
8	3,86	$5/2^+$	$1d_{5/2}$	0,015	—	—	1—2
9	3,97	$5/2^-$			—	—	0,5
10	4,36	$1/2^+$	$2s_{1/2}$	0,06	0,55	1,8±0,7	5—5,5
12	5,29	$5/2^+$	$1d_{5/2}$	(0,55)	—	—	1
18	5,99	$3/2^-$	$1p_{3/2}$	(2,0)	—	—	2
	6,5–8,5				—	—	1,5—2,0
	8,5–10,5				—	—	0,5—1,0

Levels whose population cross sections were used as the reference cross sections.

sitions listed in the second column on the left in Table V. The cross sections $\sigma(\gamma,p)_{2.6}$, $\sigma(\gamma,p)_{4.0}$, and $\sigma(\gamma,p)_{5.8}$ are divided into $\sigma(\gamma,p_f)$ in accordance with the data from $(\gamma,p\gamma')$ experiments (the averaged probabilities of the population of individual levels obtained in Refs. 48 and 49 were used). Here, as already mentioned, it was assumed that the individual $\sigma(\gamma,p_f)$ for closely spaced levels have the same energy dependence as the initial cross section for the population of this group of levels of the final nucleus.

The photoneutron cross sections were converted from the photoproton ones on the basis of Eq. (17). The values of l_{min} and l_{max} for different partial channels are given on the right-hand side of Table V (in five cases l can be determined uniquely, i.e., $l_{min}=l_{max}$). In accordance with the existing uncertainty in l we obtained the maximum and minimum values of the total photoneutron cross section $\sigma(\gamma,n)=\Sigma_f\sigma(\gamma,n_f)$.

It turns out[46] that the experimental photoneutron cross section in practically the entire energy range is quite close to the error corridor of the conversion. This indicates that, on the whole, the conversion procedure, used correctly, reproduces the ratio of the probabilities for photoproton and photoneutron emission in the DGR region for ^{24}Mg. The partial photoneutron cross sections obtained by conversion from the proton channel, combined to form the cross sections for groups of states of the final nucleus ^{23}Mg with centers of gravity shown in Table V, are also shown in Fig. 13 (solid lines) for comparison. The values of $\sigma^{int}(\gamma,n_f)$ obtained by conversion $\sigma(\gamma,p_f)\rightarrow\sigma(\gamma,n_f)$ are given in the right-most column of Table VII.

The energy dependences of the photonucleon cross sections for the population of individual levels of the final nuclei, $\sigma(\gamma,p_f)$ and $\sigma(\gamma,n_f)$, were then used to isolate the semidirect components of these cross sections and also the semidirect components of the photoproton cross section $\sigma(\gamma,p)=\Sigma_f\sigma(\gamma,p_f)$, the photoneutron cross section $\sigma(\gamma,n)=\Sigma_f\sigma(\gamma,n_f)$, and the photoabsorption cross section $\sigma_\gamma=\sigma(\gamma,p)+\sigma(\gamma,n)$. Equations (8), (9), (12), (15), and (16) were used for this.

In calculating the semidirect components of the cross sections for the population of levels of the final nuclei containing an admixture of proton holes in the $1d_{3/2}$, $1d_{5/2}$, and $2s_{1/2}$ subshells, the population cross sections respectively corresponding to the ground, first, and third excited states of ^{23}Na were used as the reference cross sections (see Table VI). The analogous neutron cross sections were used to calculate the semidirect components of $\sigma(\gamma,n_f)$.

It was assumed that these reference cross sections are formed entirely owing to semidirect DGR decay, since the corresponding populated levels of ^{23}Na and ^{23}Mg (f=0, 1, and 3) contain most (60–90%) of the spectroscopic strength of each of the three possible holes in the $1d2s$ shell of ^{24}Mg, so that these levels are close to pure hole levels. The fact that the reference cross sections selected are produced mainly by semidirect processes is also confirmed by

the results of the theoretical calculation of photodisintegration of ^{24}Mg (Ref. 45).

The (γ,p_4) and (γ,n_5) cross sections should be entirely formed by semidirect decays, since the populated final states are, respectively, pure proton and neutron holes in the $1p_{1/2}$ subshell of ^{24}Mg (the spectroscopic factors of these states exhaust the corresponding sum rule for the $1p_{1/2}$ subshell).

The hole in the $1p_{3/2}$ subshell is strongly spread out. Only an upper estimate was obtained for the partial cross sections for the population of levels containing an admixture of this hole by using the (γ,p_7) and (γ,n_7) cross sections as the reference ones.

For each partial cross section for the population of a level with nonzero spectroscopic factor the lowest and highest value of the semidirect component, $\sigma_{ph}^{\min}$ and $\sigma_{ph}^{\max}$, respectively, corresponding to emission of a nucleon with the maximum and minimum l, was calculated. The values of $l_{\min}$ and $l_{\max}$ in this calculation coincide with those given in Table V, except for the population of groups of the highest levels of the final nuclei, $\sigma(\gamma,p^n)_{7,6}$ and $\sigma(\gamma,p^n)_{9,6}$. In this case $l_{\min}=0$ and $l_{\max}=2$ were used in the calculation.

The cross sections for the reactions (γ,p_2) and (γ,n_2), (γ,p_5) and (γ,n_4), and (γ,p_8) and (γ,n_9) going to levels with $C^2S^-=0$ have zero semidirect components ($\sigma_{ph}^{\min}=\sigma_{ph}^{\max}=0$). Of the other partial channels, a significant fraction of semidirect decays is contained only in the mirror channels (γ,p_6) and (γ,n_6).

The cross sections for the reactions $(\gamma,n)_{7,6}$ and $(\gamma,n)_{9,6}$ are nearly zero, so that the absence of information about the values of S_n^- in the range $E_f=6.5-10.5$ MeV has practically no effect on the final results (in this case $\sigma_{ph}^{\min}\approx\sigma_{ph}^{\max}\approx 0$).

The upper and lower limits on semidirect components of the (γ,p) and (γ,n) cross sections and the photoabsorption cross sections were obtained by summing $\sigma_{ph}^{\min}$ and $\sigma_{ph}^{\max}$ for the individual partial cross sections. They are given in Fig. 14. Let us discuss these results. It follows from this figure that semidirect processes play an important role in the formation and decay of DGRs of ^{24}Mg. The determination of the role of semidirect processes in the integrated cross sections for photonucleon reactions reduces to the computation of the corresponding areas under the curves for the cross sections and their semidirect components. In connection with this we note that the photoproton and photoneutron cross sections given in Fig. 14 are, respectively, the cross sections for the reactions $(\gamma,p)+(\gamma,pn)$ and $(\gamma,n)+(\gamma,pn)$, and, according to Ref. 2,

$$\int_0^{30}[\sigma(\gamma,p)+\sigma(\gamma,pn)]dE_\gamma=180\pm 30\ \text{MeV}\cdot\text{mb},$$

$$\int_0^{30}[\sigma(\gamma,n)+\sigma(\gamma,pn)]dE_\gamma=76\pm 15\ \text{MeV}\cdot\text{mb}.$$

The estimate of $\int_0^{30}\sigma(\gamma,pn)dE_\gamma$ leads to a value ≈ 10 MeV · mb. Using the values of the integrated cross sections for photonucleon reactions given in Fig. 14, we easily obtain the following results: 1) the semidirect mechanism is

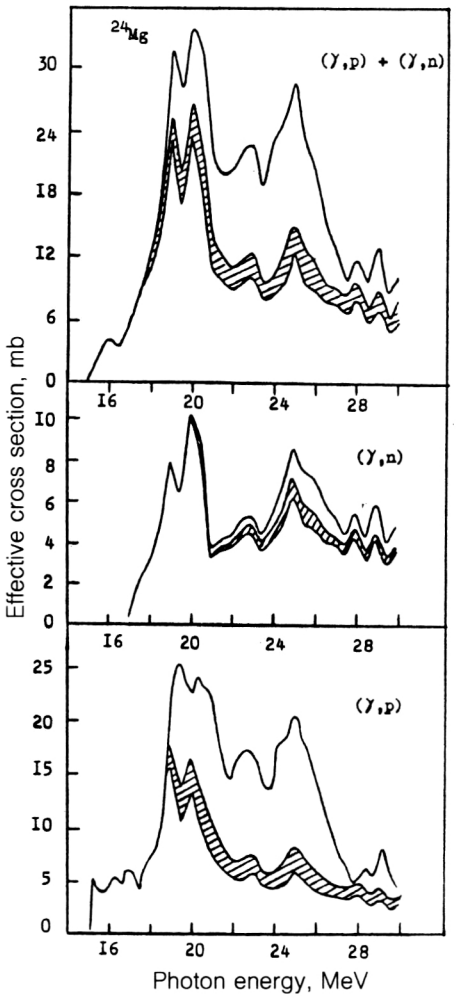

FIG. 14. Total photonucleon cross sections and photoabsorption cross sections $\sigma_\gamma\approx\sigma(\gamma,n)+\sigma(\gamma,p)$ for ^{24}Mg (solid lines) and also their semidirect components (shaded regions).

responsible for 62–73% of the total integrated cross section of the (γ,p) and (γ,n) reactions (up to $E_\gamma=30$ MeV); 2) in the (γ,p) channel the probability for semidirect processes is 47–62%; in the (γ,n) channel this probability is considerably higher: 90–95%. This situation occurs for most nuclei of the $1d2s$ shell and is related to the fact that the neutron separation energy for them is considerably (several MeV) greater than the proton separation energy. Because of this the photoneutron cross sections for the population of high-lying final levels, which in most cases have a nonhole nature, are strongly suppressed, and the total photoneutron cross sections (in contrast to the photoproton ones) are formed almost exclusively by the population of low-lying hole levels and therefore, to a greater degree, by semidirect decay.

The contribution of $E1$ transitions $A(1d2s\rightarrow 1f2p)$ to the total integrated cross section of the (γ,p) and (γ,n) reactions for ^{24}Mg is 71%. This contribution is 68% and 82% in the (γ,p) and (γ,n) channels, respectively.

The nucleus ^{27}Al

This nucleus is a convenient object for illustrating the method used to analyze the partial photonucleon cross sec-

tions. First, for it there are experimental data obtained both by γ spectrometry[14,50] and by proton spectrometry.[50,51] The results of these independent experiments agree well with each other. Second, for ^{27}Al the neecessary information from proton and neutron capture reactions is available.[13,20] Third, this nucleus is odd, so that this example is the most general one (all the expressions for the DGR semidirect decay widths for nuclei of the other type will be a special case of the expression for the odd nucleus). Fourth, in this example the hole configurations of most of the populated states belong to the single $1d_{5/2}$ subshell (according to the data on capture reactions,[13,20] the admixture of the higher $2s_{1/2}$ subshell in the ground state of ^{27}Al is less than 5%), which drastically decreases the uncertainty in the estimates of the ratios of the partial widths of semidirect decay. Therefore, the method can be checked in detail for the ^{27}Al nucleus.

In Eqs. (7)–(9) the partial cross sections $\sigma(\gamma,x_f)$ pertain to a definite excitation energy E_q of the target nucleus. In other words, to use these expressions it is necessary to know the energy dependences of the partial cross sections. In the example of ^{27}Al under consideration, owing to the absence of the energy dependences of $\sigma(\gamma,n_f)$ and the impossibility of obtaining them from the energy dependences of $\sigma(\gamma,p_f)$ by the method used above for the self-conjugate ^{24}Mg nucleus, we shall analyze only the partial photonucleon cross sections integrated over E_q, i.e.,

$$\sigma^{\text{int}}(\gamma,x_f)=\int_0^{E^m}\sigma(\gamma,x_f)dE_q. \tag{18}$$

Therefore, instead of Eqs. (7)–(9) we need to use the expressions valid for the integrated cross sections.

The DGR of ^{27}Al, as for any non-self-conjugate nucleus, is formed from two isospin components (see Fig. 15): one with $T_<=T_0$ and one with $T_>=T_0+1$, where T_0 is the isospin of the nuclear ground state (for ^{27}Al, $T_<=1/2$ and $T_>=3/2$). It is simplest to write it in the form of two states with $T_q=T_<$ and $T_>$ which absorb all the $E1$-transition probability. We shall take the energies of the centers of gravity of the corresponding isospin components to be the energies of these states, $E(T_<)$ and $E(T_>)$. We recall that we are considering only the branch of the DGR of ^{27}Al which is due to $E1$ transitions from an outer ($1d2s$) shell. In this case, according to the data of Refs. 27 and 52, for $E(T_<)$ and $E(T_>)$ we should take the values 16.5 and 20 MeV.

The isospin of the low-lying states of the final nucleus $(A-1,Z-1)$ is $T_f=T_0+1/2$. Both branches of the DGR lead to the population of these states as a result of proton emission. The isospin of the low-lying states of the nucleus $(A-1,N-1)$ is $T_f=T_0-1/2$. Therefore, only the branch $T_<=T_0$ of the DGR leads to the population of these states as a result of neutron emission. States with $T_f=T_0+1/2$ in the nucleus $(A-1,N-1)$ usually lie rather high and are reached only by the $T_>$ branch of the DGR.

This feature of DGRs in nuclei with $T_i\neq 0$ makes the expressions for the semidirect components more complicated:

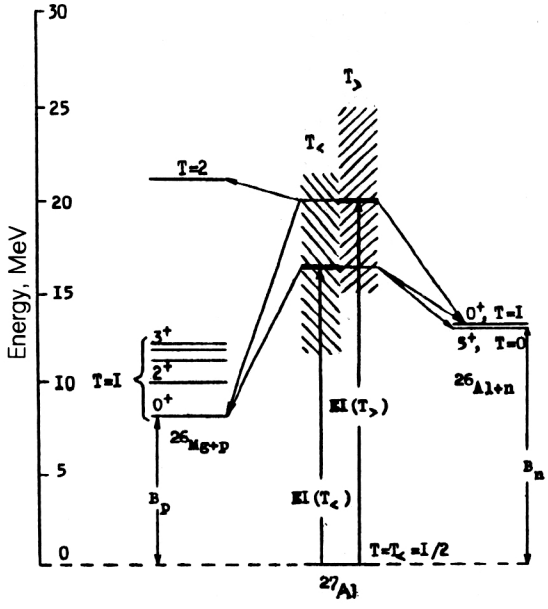

FIG. 15. Isospin components of the dipole giant resonance of ^{27}Al.

$$\sigma_{ph}(\gamma,x_f)=\begin{cases}\sigma_<\dfrac{\Gamma^{\uparrow}_<(f)}{\Gamma_>}+\sigma_>\dfrac{\Gamma^{\uparrow}_>(f)}{\Gamma_>} & \text{for } T_f=T_0-1/2\\ \sigma_>\dfrac{\Gamma^{\uparrow}_>(f)}{\Gamma_>} & \text{for } T_f=T_0+1/2,\end{cases} \tag{19}$$

where $\sigma_<$ and $\sigma_>$ are the total-absorption cross sections in the corresponding isospin branch, $\Gamma_<$ and $\Gamma_>$ are the total widths of the corresponding branch, including the width related to the spread of the doorway states over complex states, and $\Gamma^{\uparrow}_<(f)$ and $\Gamma^{\uparrow}_>(f)$ are the corresponding widths for nucleon emission into the continuum during the semidirect stage. They can be calculated by using Eq. (13). The following expression holds for the ratio of the semidirect components of the integrated cross sections of the reactions (γ,x_1) and (γ,x_2) [cf. (8)]:

$$\frac{\sigma^{\text{int}}_{ph}(\gamma,x_1)}{\sigma^{\text{int}}_{ph}(\gamma,x_2)}=\begin{cases}\dfrac{\sigma_<\Gamma^{\uparrow}_<(1)+a\sigma_>\Gamma^{\uparrow}_>(1)}{\sigma_<\Gamma^{\uparrow}_<(2)+a\sigma_>\Gamma^{\uparrow}_>(2)} & \text{for } T_f=T_0-1/2\\ \dfrac{\Gamma^{\uparrow}_>(1)}{\Gamma^{\uparrow}_>(2)} & \text{for } T_f=T_0+1/2,\end{cases} \tag{20}$$

where $a=\Gamma_</\Gamma_>$.

Satisfaction of Eq. (20) for $\sigma^{\text{int}}(\gamma,x_1)/\sigma^{\text{int}}(\gamma,x_2)$ would indicate that semidirect decay dominates in the partial cross sections being compared.

The ratio of the cross sections (probabilities) $\sigma_<$ and $\sigma_>$ will be taken from theory. According to Ref. 53,

$$\frac{\sigma_<}{\sigma_>}\approx\frac{1}{T_0}\left(\frac{1-1.5T_0A^{-2/3}}{1+1.5A^{-2/3}}\right)$$

and the ratio for aluminum is 0.35:0.65.

The quantity $a=\Gamma_{<}/\Gamma_{>}$ is unknown and is a parameter in the analysis of the experimental data.

Let us give the proton and neutron populations of the outer $1d_{5/2}$ and $2s_{1/2}$ subshells needed for the calculations and the total numbers of nucleons in these subshells [see (13) and (14)]:

$$\nu_{d_{5/2}}(n)=0.92, \quad \nu_{d_{5/2}}(p)=0.83, \quad \nu_{s_{1/2}}(n)=0.25,$$

$$\nu_{s_{1/2}}(p)=0.01, \quad N_{d_{5/2}}=10.48, \quad N_{s_{1/2}}=0.52.$$

Using the fact that in the ground state of ^{27}Al practically all the nucleons of the outer $1d2s$ shell are located in the $1d_{5/2}$ subshell, in the calculations we shall neglect the admixture of the higher $2s_{1/2}$ subshell, which, as seen from the above numbers, is less than 5%. Even for the levels of the final nucleus ^{26}Al, which contained a significant part of the spectroscopic strength of the $2s_{1/2}$ hole, it was assumed that the partial cross sections arise from the presence of an admixture of only the $1d_{5/2}$ hole. The results obtained below confirm the validity of this assumption.

The widths $\Gamma^{\uparrow}_{<}$ and $\Gamma^{\uparrow}_{>}$ contain the sums $\Sigma_{\alpha}P_{\alpha}X^2_{\alpha\beta}(q)$. Since we are considering only transitions of nucleons from the $1d_{5/2}$ subshell to the $1f2p$ shell, these sums can be written as

$$\sum_{\alpha} P_{\alpha}X^2_{\alpha\beta}=P_1X^2_1+P_3X^2_3,$$

where

$$X^2_1=X^2_{d_{5/2}p_{3/2}}, \quad X^2_3=X^2_{d_{5/2}f_{7/2}}+X^2_{d_{5/2}f_{5/2}},$$

and P_1 and P_3 are the barrier penetration factors for nucleons with orbital angular momentum 1 and 3.

The ratio (20) depends on the degree of mixing in the orbital angular momentum, i.e., on the relation between the coefficients X_1 and X_3 in the wave function of both the $T_{<}$ and the $T_{>}$ dipole states. In the calculations the degree of mixing in the orbital angular momentum for each of these states was varied independently, using the parameter

$$b=\frac{X^2_3}{X^2_1+X^2_3},$$

i.e., two parameters $b_{<}$ and $b_{>}$ were used. Here it was assumed that $X^2_1(T_{<})+X^2_3(T_{<})\approx X^2_1(T_{>})+X^2_3(T_{>})$. This condition is satisfied for dipole states whose wave function is dominated by the same particle–hole configurations [in this case $1d^{-1}_{5/2}(1f2p)^1$]. The differences in the structure of the wave functions of the $T_{<}$ and $T_{>}$ states arising from violation of this condition lead to a change of the constant a.

The large amount of experimental data avaliable on the cross sections of the (γ,p_f) and (γ,n_f) reactions for ^{27}Al makes it possible to study the effect of the parameters a, $b_{<}$, and $b_{>}$ on the predicted values of $\sigma^{\rm int}_{ph}(\gamma,x_f)$ in detail and to choose fairly unambiguously the values of the parameters which best describe the experimental results.

The partial cross sections $\sigma^{\rm int}(\gamma,p_f)$ and $\sigma^{\rm int}(\gamma,n_f)$ for the ^{27}Al nucleus obtained in the experiments of Refs. 14, 50, and 51 are given in Tables VIII and IX together with the spectrometric characteristics of the populated states[13,20] and the values of $\sigma^{\rm int}_{ph}(\gamma,p_f)$ and $\sigma^{\rm int}_{ph}(\gamma,n_f)$ (right-hand columns of the table). The range of ^{27}Al excitation energies studied reaches 30 MeV. Therefore, the entire DGR region is essentially covered.

The data of the various experiments can be compared only for (γ,p_f) channels (Table VIII). We see that the data of the experiments of Refs. 14, 50, and 51 on the whole are in fairly good agreement with each other. Population of the ^{26}Mg levels up to $E_f=7.25$ MeV is observed in the most complete $(\gamma,p\gamma')$ experiment.[14] These levels have positive parity, and the spectroscopic strength of the proton hole excitations in the outer $(1d2s)$ shell of ^{27}Al is practically exhausted by these levels. Therefore, the dipole transitions observed in $(\gamma,p\gamma')$ experiments completely pertain to group A $(1d2s\rightarrow 1f2p)$.

The photoproton spectrometry experiment of Ref. 51 allows all the $E1$ transitions to be distinguished, and the (γ,p_f) cross sections for the population of ^{26}Mg levels with $E_f>7.5$ MeV are due to DGR decays of group B $(1p\rightarrow 1d2s)$. This range of E_f in Table VIII corresponds to three partial cross sections for the population of groups of ^{26}Mg levels with centers of gravity $\bar{E}_f$ equal to 8.5, 11, and 13 MeV. It follows from the hole nature of the populated levels that the first of these ($\bar{E}_f=8.5$ MeV) is due to DGR decay of the $1p_{1/2}\rightarrow 1d2s$ branch. The other two ($\bar{E}_f=11$ and 13 MeV) are due to DGR decay of the $1p_{3/2}\rightarrow 1d2s$ branch.

On the whole, the (γ,n_f) transitions (Table IX) completely pertain to branch A of the DGR. Using the estimates of $\sigma^{\rm int}_{ph}(\gamma,n_f)$ for $f=0$, 1, and 2 (details below), the neutron channels given in this table completely exhaust the cross section $\sigma^{\rm int}(\gamma,n)$ for ^{27}Al. Therefore, ^{26}Al levels with $E_f>5$ MeV should not be populated in the reaction ^{27}Al$(\gamma,n)^{26}$Al, and branch B of the DGR is completely absent.

Let us return to the procedure for estimating $\sigma^{\rm int}_{ph}(\gamma,x_f)$. As the reference partial cross section [the cross section from which all the other $\sigma^{\rm int}_{ph}(\gamma,x_f)$ are calculated] we chose the cross section for population of the ^{26}Mg level with energy 1.81 MeV, i.e., the cross section for the (γ,p_1) reaction. This choice was made for the following reasons. First, the cross section for this reaction is formed by semidirect processes.[27,33] We note that the analog of the 1.81-MeV level in ^{26}Mg is the 2.07-MeV level of ^{26}Al. Second, the absolute value of $\sigma^{\rm int}(\gamma,p_1)$ is known most accurately (about 10%). It has been determined in several independent experiments (Refs. 14, 50, and 51), and the data of these agree within the experimental error.

The values of $\sigma^{\rm int}_{ph}(\gamma,p_f)$ and $\sigma^{\rm int}_{ph}(\gamma,n_f)$ given in Tables VIII and IX correspond to $b_{>}=1$. For this $b_{>}$ and any a, by varying $b_{<}$ it is possible to reproduce simultaneously not only the observed integrated cross sections of (γ,n_f) reactions for $T=0$ levels with energies 1.06, 1.76, 2.37, and 2.55 MeV, but also the integrated cross section for the population of the 2.07-MeV $(T=1)$ level in the neutron channel. This indicates that the population of these levels occurs primarily owing to semidirect processes [Eq. (20)

TABLE VIII. Integrated cross sections of $^{27}Al(\gamma,p_f)^{26}Mg$ reactions and characteristics of populated levels of ^{26}Mg (Refs. 13 and 20).

Xa	Level characteristics of ^{26}Mg				$\sigma^{int}(\gamma, p_f)$, MeV · mb			$\sigma^{int}_{ph}(\gamma, p_f)$
f	E_f, MeV	J^π	nl_j	C^2S^-	$\gamma, p\gamma'$ [14] E^m=32 MeV	$\gamma, p\gamma'$ [50] E^m=24 MeV	γ, p [51] E^m=29,7 MeV	
0	0	0^+	$1d_{5/2}$	0,29	—	—	10	10,6
1	1,81	2^+	$1d_{5/2}$	1,07	22±4	25±6	28	22*
2	2,94	2^+	$2s_{1/2}$ 0,02; $1d_{5/2}$ 0,28		5,3±2,5	9,3±2	24	3,5
3	3,59	0^+	$1d_{5/2}$	0,01	<1,4	(4±1,3)		<0,13
4	3,94	3^+	$2s_{1/2}$ 0,01; $1d_{5/2}$ 0,03		2,6±1,3			<0,25
5	4,31	4^+			32±5	19±2,5		
6	4,33	2^+	$1d_{5/2}$	1,9		<3,1		11,4
7	4,35	3^+			5,7±2,5	6,3±2,5		
8	4,83	4^+					63	
9	4,90	2^+	$1d_{5/2}$	0,36	<7,7	7,9±2		1,5
10	4,97	0^+			1,8±0,6	<2,5		
11	5,29	2^+			1,8±0,6			0
12	5,47	4^+	$1d_{5/2}$	0,32	4,5±1,3			0,9
15	6,13	$(2,3)^+$	$1d_{5/2}$	0,14				
—	7,25		$1d_{5/2}$	0,34			32	0,4
	$\bar{E}_f$=8,5		$1p_{1/2}$	2,62–3,1			24	0–24
	$\bar{E}_f$=11		$1p_{3/2}$				16	
	$\bar{E}_f$=13		$1p_{3/2}$				12	

Cross section used as the reference.

holds for their experimental cross sections]. The cross sections $\sigma^{int}_{ph}(\gamma,n_f)$ for the $T=1$ levels of ^{26}Al with energies 3.16 and 4.71 MeV (the analogs of the 2.94- and 4.31-MeV levels of ^{26}Mg) are lower than the observed values, which may be explained by the presence in these channels of not only semidirect, but also statistical processes. On the whole, the population of the 2.66-MeV level can be attributed to non-semidirect processes. In Table VII we also give the values of $\sigma^{int}_{ph}(\gamma,n_f)$ for the three lowest levels ($f=0$, 1, and 2) of the ^{26}Al nucleus, for which there are no experimental data. These values, as will be seen below, should be viewed as estimates of the cross sections for the population of these levels.

We stress that the experimental value of the cross section for the population of the 2.06-MeV level of ^{26}Al admits a single value of the parameter $b_>$, namely, $b_>=1$. This value of $b_>$ corresponds to the case where the $T_>$ state decays with the emission of nucleons with only $l=3$. As $b_>$ decreases, $\sigma^{int}_{ph}(\gamma,n_7)$ [when $\sigma^{int}(\gamma,n_f)$ is reproduced for levels of the final nucleus with zero isospin] grows, rapidly diverging from the experimental value. Even the introduction of a small admixture of nucleon decays with $l=1$ into the $T_>$ branch of the DGR of ^{27}Al leads to a sharp increase of $\sigma^{int}_{ph}(\gamma,n_7)$ and causes the calculated value to be considerably larger than the experimental one. Such versions of the calculation should be discarded, since the semidirect component of the cross section cannot be larger than the observed cross section, to which all possible forms of statistical decay contribute, in addition to semidirect decay.

Therefore, we used $b_>=1$. The parameters a and $b_<$ were varied in order to obtain the best agreement with experiment. It turned out (the corresponding data are given in Ref. 36) that the calculated values of the cross sections for the population of ^{26}Al levels closest to experiment varied only slightly with a (particularly for the 1.06, 1.76, 1.85, 2.37, and 2.55 MeV levels). In Table IX we give $\sigma^{int}_{ph}(\gamma,n_f)$ for three sets of parameters a and $b_<$ ($b_>=1$). The values of $\sigma^{int}_{ph}(\gamma,p_f)$ in Table VIII are given for $b_>=1$ only for one set of a and $b_<$ (0.2 and 0.94), since the

TABLE IX. Integrated cross sections of $^{27}Al(\gamma,n_f)^{26}Al$ reactions, their semidirect components, and characteristics of populated levels of ^{26}Al (Refs. 13 and 20).

Level characteristics of ^{26}Al					$\sigma^{int}(\gamma, n_f)$, MeV · mb	$\sigma^{int}_{ph}(\gamma, n_f)$, MeV · mb		
f	E_f, MeV	$J^\pi;T$	nl_j	C^2S^-	$\gamma, n\gamma'$ [14] E^m=32,0 MeV	a = 0,1 $b_<$ = 0,965	a = 0,2 $b_<$ = 0,94	a = 1 $b_<$ = 0,72
0	0	$5^+;0$	$1d_{5/2}$	1,1		99	83	65
1	0,23	$0^+;1$	$1d_{5/2}$	0,16		8,9	10,4	11,9
2	0,42	$3^+;0$	$2s_{1/2}$ $1d_{5/2}$	0,15 0,10		7,3	6,2	5,1
3	1,06	$1^+;0$	$1d_{5/2}$	0,30	13,7±2	13,8	12,9	12,2
4	1,76	$2^+;0$	$2s_{1/2}$ $1d_{5/2}$	0,02 0,06	1,6±0,9	1,6	1,6	1,7
5	1,85	$1^+;0$	$1d_{5/2}$	0,04		1	1	1,1
6	2,069	$4^+;0$						
7	2,07	$2^+;1$	$1d_{5/2}$	0,53	11,7±1	11,8	14,1	16,6
8	2,072	$1^+;0$						
9	2,37	$3^+;0$	$1d_{5/2}$	0,36	4,0±0,8	5,4	5,8	6,3
10	2,55	$3^+;0$	$1d_{5/2}$	0,36	6,8±1,9	4,3	4,6	5,1
11	2,66	$2^+;0$			6±1,3			
13	2,91	$2^+;0$	$2s_{1/2}$ $1d_{5/2}$	0,007 0,06		0,25	0,25	0,25
15	3,16	$2^+;1$	$2s_{1/2}$ $1d_{5/2}$	0,02 0,14	2,3±0,5	1,3	1,6	1,9
16	3,40	$5^+;0$	$1d_{5/2}$	0,19		0	0	0
20	3,68	$3^+;0$	$2s_{1/2}$ $1d_{5/2}$	0,02 0,18		0	0	0
25	3,96	$3^+;0$	$2s_{1/2}$ $1d_{5/2}$	0,05 0,10		0	0	0
35	4,71	$4^+;1$	$1d_{5/2}$	1,07	10,7±2,5	1,9	2,4	2,8

$\sigma^{int}_{ph}(\gamma,p_f)$ also vary insignificantly for the relation between a and $b_<$ giving the best agreement with experiment.

Moreover, the data only on the proton decay channel of the DGR of ^{27}Al turned out to be completely insensitive to the choice of parameters a, $b_<$, and $b_>$. In all the versions of the calculation using $\sigma^{int}(\gamma,p_1)$ as the reference cross section, the cross sections for the reactions (γ,p_0) and (γ,p_1) can be attributed almost entirely to semidirect decays. For the other (γ,p_f) the fraction of semidirect decays is less than unity and decreases with increasing f.

We conclude this section by estimating the probability of $E1$ transitions of branch A of the DGR for ^{27}Al along with the probability for semidirect processes. All the estimates will pertain to the region $E_\gamma < 30$ MeV.

It follows from Table VIII that for branch A of the DGR, $\Sigma_f\sigma^{int}(\gamma,p_f)=157$ MeV · mb. Using the fact that $\int_0^{30}\sigma(\gamma,p)dE_\gamma=180$ MeV · mb for ^{27}Al, we find that the fraction of branch A of the DGR in the photoproton channel is 0.87. For the (γ,p) channel branch B of the DGR is entirely due to the partial cross section for the population of the group of ^{26}Mg levels with $\bar{E}_f=8.5$ MeV, i.e., $1p_{1/2}\to 1d2s$ transitions. The partial cross sections for the population of the groups of ^{26}Mg levels with $\bar{E}_f=11$ and 13 MeV, which are unstable with respect to subsequent neutron emission, form the cross section of the reaction $^{27}Al(\gamma,pn)^{25}Mg$, for which $\int_0^{30}\sigma(\gamma,pn)dE_\gamma\approx 30$ MeV · mb. The cross section $\sigma(\gamma,pn)$ for ^{27}Al is formed by $1p_{3/2}\to 1d2s$ transitions.

The probability for semidirect processes in the (γ,p) channel is estimated to be

$$\mathscr{P}_p=\frac{\Sigma_f\sigma^{int}_{ph}(\gamma,x_f)}{\int_0^{E^m}\sigma(\gamma,x)dE_\gamma}, \tag{21}$$

where $x=p$ and $E^m=30$ MeV. It follows from Table VIII that $\Sigma_f\sigma^{int}_{ph}(\gamma,p_f)$ = 50–75 MeV · mb, which gives 0.28–0.42 for the estimated probability.

Since the data of Table IX exhaust all the neutron transitions, we can estimate the probability for semidirect processes in the photoneutron channel as

$$\mathscr{P}_n=\frac{\Sigma_f\sigma^{int}_{ph}(\gamma,x_f)}{\Sigma_f\sigma^{int}(\gamma,x_f)}, \tag{22}$$

where $x=n$. This gives $\mathscr{P}_n\approx 0.88$. We recall that the cross section for the reaction $^{27}Al(\gamma,n)^{26}Al$ is entirely due to branch A of the DGR.

Using the fact that for ^{27}Al we have $\int_0^{30}\sigma(\gamma,n)dE_\gamma=130$ MeV · mb, from these numbers we easily obtain the probability for semidirect processes in the total integrated cross section for the reactions (γ,p) and (γ,n). It is 0.53–0.62. The fraction of transitions of group A in $\sigma(\gamma,p+\gamma,n)$ is 0.92.

CONCLUSION

Let us summarize our results. The data of $(\gamma,x\gamma')$ experiments that we have analyzed for the examples of three nuclei show that this method of studying highly excited nuclear states, in particular, DGRs, is very effective. In spite of certain complexities in the analysis and interpretation of the γ spectra, it is possible to obtain detailed information about the mechanism of photonuclear processes and about the role of nucleons of various shells in the formation of high-lying collective excitations. This method is especially informative when used in conjunction with the results of particle-spectrometry experiments.

At present the most complete $(\gamma,x\gamma')$ data are available for nuclei of the $1d2s$ shell. The partial photonuclear transitions have been measured for 15 nuclei of this region (see Table IV). Here the total number of partial nucleon channels studied is about 300. *It is therefore appropriate to analyze these data for the entire shell and to find the general regularities.* The result of this enormous analytical undertaking should be the subject of a separate publication. It should be noted that the quality of the interpretation of the data will improve if in future experiments the *measurement of the angular distributions of photonucleons in partial transitions* will be possible. Knowledge of the angular momentum allows the experimental data to be analyzed with greater certainty. However, even in the absence of information about the angular distributions, the realization of a program for an entire shell like that carried out here for three nuclei will allow deeper understanding of the nature of DGRs in light nuclei.

It is important *to increase the accuracy of measuring the partial transitions to hole levels of an outer shell* and to measure the dependence of $\sigma(\gamma,x_f)$ on the energy of the photons incident on the target nucleus. Increased measurement accuracy would make it possible to select decays from different regions of the giant resonance to different hole states. This is the *configuration splitting of dipole transitions of nucleons inside a band connected to nucleons of outer shells.*

Obtaining the partial photonuclear cross sections and particularly their energy dependences is a very important area in experimental research. The photoproton channel has been studied more completely. In this review we did not mention the fact that the probability of semidirect processes in the photoneutron channel of nuclei of the $1d2s$ shell is considerably higher than that in the photoproton channel. This means that the photoneutron branch of the DGRs of these nuclei has a better "memory" of the configuration structure of the doorway dipole states than the photoproton channel does.

Despite all the deficiencies in the data listed above, we shall significantly extend our ideas about the giant resonance in $1d2s$-shell nuclei. This can be done by using modern high-current accelerators.

[1] L. S. Cardman, Nucl. Phys. **A354**, 173c (1981).
[2] R. A. Eramzhyan, B. S. Ishkhanov, I. M. Kapitonov, and V. G. Neudatchin, Phys. Rep. **136**, 229 (1986).
[3] V. V. Varlamov, B. S. Ishkhanov, I. M. Kapitonov *et al.*, *Photonuclear Data. $(\gamma,x\gamma')$ Reactions* [in Russian] (Moscow State University Press, Moscow, 1985).
[4] U. R. Arzibekov, A. S. Gabelko, M. Kh. Zhalilov *et al.*, Izv. Akad. Nauk SSSR, Ser. Fiz. No. 2, 52 (1986) [Bull. Acad. Sci. USSR, Phys. Ser.].
[5] A. S. Gabelko, K. M. Irgashev, B. S. Ishkhanov *et al.*, Yad. Fiz. **44**, 1145 (1986) [Sov. J. Nucl. Phys. **44**, 741 (1986)].
[6] P. J. Ryan and M. N. Thompson, Nucl. Phys. **A457**, 1 (1986).
[7] A. S. Gabelko, M. Kh. Zhalilov, B. S. Ishkhanov *et al.*, Vestn. Mosk. Univ. Ser. Fiz. Astron. **27**, 43 (1986) [in Russian].
[8] U. R. Arzibekov, A. S. Gabelko, M. Kh. Zhalilov *et al.*, Yad. Fiz. **45**, 907 (1987) [Sov. J. Nucl. Phys. **45**, 562 (1987)].
[9] U. R. Arzibekov, A. S. Gabelko, M. Kh. Zhalilov *et al.*, Izv. Akad. Nauk SSSR, Ser. Fiz. **51**, 134 (1987) [Bull. Acad. Sci. USSR, Phys. Ser.].
[10] G. V. O'Rielly, D. Zubanov, and M. N. Thompson, Phys. Rev. C **40**, 59 (1989).
[11] R. Henck, P. Siffert, and A. Coche, Nucl. Instrum. Methods **60**, 343 (1968).
[12] U. R. Arzibekov, Candidate's Dissertation, Nuclear Physics Institute, Moscow State University, Moscow, 1987 [in Russian].
[13] P. M. Endt and C. Van der Leun, Nucl. Phys. **A310**, 1 (1978).
[14] U. R. Arzibekov, A. S. Gabelko, M. Kh. Zhalilov *et al.*, Yad. Fiz. **40**, 1121 (1984) [Sov. J. Nucl. Phys. **40**, 713 (1984)].
[15] V. B. Zlokazov, Comput. Phys. Commun. **28**, 27 (1982).
[16] J. T. Caldwell, S. C. Fultz, and R. L. Bramblett, Phys. Rev. Lett. **19**, 447 (1967).
[17] A. S. Gabelko, B. S. Ishkhanov, I. M. Kapitonov *et al.*, *Study of Partial Photodisintegration Channels of Nuclei in $(\gamma,x\gamma')$ Experiments* [in Russian], All-Union Institute of Scientific and Technical Information Depositor No. 7158-B85, 1985.
[18] B. S. Ishkhanov, I. M. Kapitonov, V. I. Mokeev, and I. M. Piskarev, Preprint No. 13/1985, Physics Faculty, Moscow State University, Moscow (1985) [in Russian].
[19] D. Brajnik, D. Jamnik, G. Kernel *et al.*, Phys. Rev. C **9**, 1901 (1974).
[20] P. M. Endt, At. Data Nucl. Data Tables **19**, 23 (1977).
[21] C. P. Wu, J. E. E. Baglin, F. W. K. Kirk, and T. W. Phillips, Phys. Lett. **29B**, 359 (1969).
[22] B. S. Ishkhanov, V. I. Mokeev, Yu. A. Novikov *et al.*, Yad. Fiz. **32**, 885 (1980) [Sov. J. Nucl. Phys. **32**, 455 (1980)]; A. I. Gutiĭ, Candidate's Dissertation, Nuclear Physics Institute, Moscow State University, Moscow, 1982 [in Russian].
[23] B. S. Ishkhanov, I. M. Kapitonov, V. I. Shvedunov *et al.*, Yad. Fiz. **33**, 581 (1981) [Sov. J. Nucl. Phys. **33**, 303 (1981)].
[24] J. E. M. Thomson, M. N. Thompson, and R. J. Stewart, Nucl. Phys. **A290**, 14 (1977).
[25] V. V. Varlamov, B. S. Ishkhanov, I. M. Kapitonov *et al.*, Yad. Fiz. **28**, 590 (1978) [Sov. J. Nucl. Phys. **28**, 302 (1978)].
[26] J. E. M. Thomson and M. N. Thompson, Nucl. Phys. **A330**, 66 (1979).
[27] I. M. Kapitonov, Yad. Fiz. **37**, 569 (1983) [Sov. J. Nucl. Phys. **37**, 338 (1983)].
[28] I. Rotter, Fiz. Elem. Chastits At. Yadra **15**, 762 (1984) [Sov. J. Part. Nucl. **15**, 341 (1984)].
[29] I. Rotter, Fiz. Elem. Chastits At. Yadra **6**, 435 (1975) [Sov. J. Part. Nucl. **6**, 175 (1975)].
[30] B. S. Ishkhanov, I. M. Kapitonov, V. G. Kanzyuba *et al.*, Nucl. Phys. A **405**, 287 (1983).
[31] B. S. Ishkhanov, V. G. Kanzyuba, and V. N. Orlin, Yad. Fiz. **40**, 9 (1984) [Sov. J. Nucl. Phys. **40**, 5 (1984)].
[32] J. E. M. Thomson and M. N. Thompson, Nucl. Phys. **A285**, 84 (1977).
[33] I. M. Kapitonov, Doctoral Dissertation, Nuclear Physics Institute, Moscow State University, Moscow, 1983 [in Russian].
[34] D. Ryckbosch, E. Van Camp, R. Van de Vyver *et al.*, Phys. Rev. C **26**, 448 (1982).
[35] R. L. Gulbranson, L. S. Cardman, A. Doron *et al.*, Phys. Rev. C **27**, 470 (1983).
[36] U. R. Arzibekov, A. S. Gabelko, M. Kh. Zhalilov *et al.*, Yad. Fiz. **42**, 1059 (1985) [Sov. J. Nucl. Phys. **42**, 668 (1985)].
[37] N. W. Tanner, Nucl. Phys. **63**, 383 (1965).
[38] P. P. Singh, R. E. Segel, L. Meyer-Schützmeister *et al.*, Nucl. Phys. **65**, 577 (1965).
[39] R. C. Bearse, L. Meyer-Schützmeister, and R. E. Segel, Nucl. Phys. **A116**, 682 (1968).
[40] L. Meyer-Schützmeister, Z. Vager, R. E. Segel, and P. P. Singh, Nucl. Phys. **A108**, 180 (1968).

[41] W. M. Mason, N. W. Tanner, and G. Kernel, Nucl. Phys. **A138**, 253 (1969).
[42] E. M. Diener, J. F. Amann, and P. Paul, Phys. Rev. C **7**, 695 (1973).
[43] U. R. Arzibekov, B. S. Ishkhanov, I. M. Kapitonov, and I. M. Piskarev, Yad. Fiz. **44**, 1124 (1986) [Sov. J. Nucl. Phys. **44**, 727 (1986)].
[44] V. G. Kanzyuba, Candidate's Dissertation, Nuclear Physics Institute, Moscow State University, Moscow, 1983 [in Russian].
[45] N. A. Bogdanova, A. N. Gal'tsov, B. S. Ishkhanov, and V. N. Orlin, Vestn. Mosk. Univ. Ser. Fiz. Astron. **28**, 16 (1987).
[46] K. M. Irgashev, B. S. Ishkhanov, and I. M. Kapitonov, Nucl. Phys. **A483**, 109 (1988).
[47] V. V. Varlamov, B. S. Ishkhanov, and I. M. Kapitonov *et al.*, Yad. Fiz. **30**, 1185 (1979) [Sov. J. Nucl. Phys. **30**, 617 (1979)].
[48] P. J. Ryan, M. N. Thompson, K. Shoda, and T. Tanaka, Nucl. Phys. **A411**, 105 (1983).
[49] K. Bangert, U. E. P. Berg, G. Junghans *et al.*, Nucl. Phys. **A261**, 149 (1976).
[50] P. J. Ryan, M. N. Thompson, K. Shoda, and T. Tanaka, Nucl. Phys. **A371**, 318 (1981).
[51] B. S. Ishkhanov, I. M. Kapitonov, V. I. Shvedunov, and A. V. Shumakov, Yad. Fiz. **33**, 865 (1981) [Sov. J. Nucl. Phys. **33**, 453 (1981)].
[52] R. O. Akyüz and S. Fallieros, Phys. Rev. Lett. **27**, 1016 (1971).
[53] S. Fallieros and B. Goulard, Nucl. Phys. **A147**, 593 (1970).
[54] K. Bangert, U. E. R. Berg, K. Wienhard, and H. Wolf, Z. Phys. A **278**, 295 (1976).
[55] B. J. Thomas, A. Buchnea, J. D. Irish, and K. G. McNeil, Can. J. Phys. **50**, 3085 (1972).
[56] L. Zalcman, J. E. M. Thomson, and M. N. Thompson, in *Proc. of the Intern. Conf. on Photonuclear Reactions and Applications*, Asilomar, 1973, Summaries of Contributed Papers, p. 2B12-1.

Translated by Patricia A. Millard